

## Textures in hexatic films of nonchiral liquid crystals: Symmetry breaking and modulated phases

Joseph E. MacLennan\* and Ulrich Sohling†

*Institute of Physical Chemistry, University of Mainz, D-55099 Mainz, Federal Republic of Germany*

Noel A. Clark

*Condensed Matter Laboratory, Department of Physics, University of Colorado, Boulder, Colorado 80309-0390*

Michael Seul

*AT&T Bell Laboratories, Murray Hill, New Jersey 07974*

(Received 4 November 1993)

Novel modulated textures, such as stripes and multiarmed star defects, have been observed in freely suspended films of nonchiral liquid crystals just below the smectic-*C* to hexatic phase transition. Detailed studies using depolarized reflection microscopy suggest that the stripes are locally chiral surface splay domains of the smectic-*L* phase, a tilted hexatic not previously identified in thermotropic liquid crystals. Line defects which form additional domain walls in the hexatic lattice lead to characteristic modulations of the basic one-dimensional stripe pattern. Inside thick circular islands, for example, stripes form circumferentially and the lines form centered 12-armed stars, resulting in a regular arrangement of hexatic domains in the form of a brick wall pattern. The observation that line defects which are not pinned at the film boundaries always form closed loops supports a model of the stripe pattern based on local chiral symmetry breaking.

PACS number(s): 61.30.Eb, 64.70.Md, 68.15.+e, 75.70.Kw

### I. INTRODUCTION

Many low-dimensional systems exhibit unidirectionally modulated (stripe domain) states whose characteristic modulation period is set by the balance of a short-range attractive "domain wall" energy and a long-range, repulsive interaction which may be magnetostatic, electrostatic, or elastic in origin. Such systems include, for example, magnetic and organic thin films [1,2] as well as stress domains on certain semiconductor and metal surfaces [3]. Stripe textures are also observed in freely suspended liquid crystal films. In particular, their appearance in films made of *chiral* materials is well documented and may be understood in the framework of competing interactions outlined above [4-7].

We recently reported the observation and initial characterization of modulated textures in thermotropic liquid crystal (LC) films composed of *nonchiral* materials [8]. In particular, we described the formation of a stable, macroscopic texture of alternating uniform stripes whose appearance is strikingly similar to textures predicted to occur under particular boundary conditions in the smectic-*L* phase, a hexatic phase which has so far been positively identified only in a single lyotropic LC system [9]. The present paper contains a general analy-

sis of the symmetry of tilted smectic films and a detailed exposition of our experimental observations. In particular, we describe temperature-induced transitions between different kinds of linear modulated phases, report the transformation of 12- to six-armed star defects in circular islands, and describe the response of the films to applied electric and magnetic fields. Finally, we explore the implications of chirality for the topology of linear domain boundaries in these films.

Freely suspended films, which may be from one to several hundred smectic layers thick, are a unique preparation for studying the physics of LC in two dimensions [10]. Their substrate-free geometry enables the direct observation of many otherwise inaccessible structural transitions, by a variety of experimental techniques. Our efforts have focused on the observation and interpretation of optical textures in tilted smectic phases of pure (i.e., single-compound), nonchiral LC materials. The LC phases relevant to these studies are described briefly below.

In general, the highest-temperature tilted phase is the smectic-*C* (SC) phase. In this phase, the director is tilted away from the layer normal  $\hat{z}$  by a temperature-dependent angle  $\psi$  (typically  $\psi \sim 20^\circ$ ) but is otherwise free to orient anywhere on the so-defined "tilt cone." The director orientation field can be described in two dimensions either by the *c*-director field  $\hat{c}(x, y)$  obtained by projecting the director  $\hat{n}(x, y)$  onto the smectic layer plane, or, equivalently, by the azimuthal orientation of the *c* director,  $\phi(x, y)$ , as shown in Fig. 1(a). The in-plane positional ordering of the molecules in the SC is liquidlike.

At lower temperatures, there exist the tilted hexatic

\*Present address: Condensed Matter Laboratory, Department of Physics, University of Colorado, Boulder, CO 80309-0390.

†Present address: Department of Polymer Chemistry, Groningen University, Nijenborgh 4, 9747 AG Groningen, The Netherlands.

phases, a class which includes the smectic *I* (SI), smectic *F* (SF), and smectic *L* (SL). These phases exhibit bond-orientational ordering and are more viscous and elastically stiffer than the SC [11]. In the SI and SF phases, the molecules are tilted, respectively, toward the nearest and next-nearest neighbors of their local pseudo-hexagonal lattice, as indicated in Fig. 1. The *c*-director orientation in the SL phase is locked along a direction *intermediate* between SI and SF, the offset from the molec-

ular bond direction being a particular angle in the range  $0 < |\phi_L| \lesssim 30^\circ$ . While the orientational ordering in the SI and SF is sixfold degenerate, we note that bulk SL material has, in general, a *twelvefold* orientational degeneracy. This is because there is a pair of SL substates, (SL<sub>1</sub>, SL<sub>2</sub>), arranged symmetrically about each of the six bond directions. The height of the energy barrier between adjacent SL<sub>1</sub> and SL<sub>2</sub> states depends on whether a bond direction separates them or not, as indicated in Fig. 1(b). The SL phase is predicted to occur in thermotropic LC at temperatures intermediate between SI and SF. Although the positional ordering of the molecules is still short range (liquidlike) in these hexatic phases, the director orientation is now coupled to the bond-orientational order, which is quasi-long-range.

This concludes our introduction to the tilted smectic phases. In the next section of the paper (Sec. II), we present a general discussion of modulated phases in liquid crystal films. In Sec. III we describe the techniques and materials used in our experiments. This is followed in Sec. IV by a detailed summary of the fundamental experimental observations. In Sec. V we develop a model of the stripe phase, which we then apply to chiral line defects in Sec. VI. The model is then reviewed in the light of additional experimental data and relevant theoretical considerations (Sec. VII). The paper concludes with a general summary (Sec. VIII).

## II. MODULATED PHASES IN FREELY SUSPENDED FILMS

### A. General symmetry considerations

As we will show, the smectic-*L* films studied here spontaneously break up into stripe domains which are structurally equivalent but differ by the sign of an internal order parameter. In order to understand the origin of this behavior, it is useful to analyze the symmetries of tilted SC, SI, SF, and SL films.

Modulated textures in freely suspended films were first reported in tilted phases of *chiral* LC [4,12]. Such materials are intrinsically ferroelectric, exhibiting a spontaneous, in-plane polarization **P** along the phase's only symmetry element, a *C*<sub>2</sub> axis oriented perpendicular to the tilt plane  $\hat{z}$ - $\hat{n}$  and hence also perpendicular to  $\hat{c}$  [13]. These modulations can be accounted for by continuum elastic theories which treat **P** as a vector order parameter and predict the spontaneous formation of parallel bands of polarization splay (*c*-director bend) in such ferroelectric films [5-7].

In general, tilted phases, such as the SC and SI, which are composed of nonchiral molecules possess, in addition to the aforementioned *C*<sub>2</sub> axis, a reflection plane,  $\sigma$ , which is congruent with the tilt plane as illustrated in Fig. 1(a). The combination of these two symmetry elements, i.e., a proper rotation followed by reflection through a plane perpendicular to the rotation axis, is equivalent to an improper rotation. That is, in tilted phases of nonchiral molecules there exists an improper axis, *S*<sub>2</sub>, perpendicular to the tilt plane, and hence an inversion center.

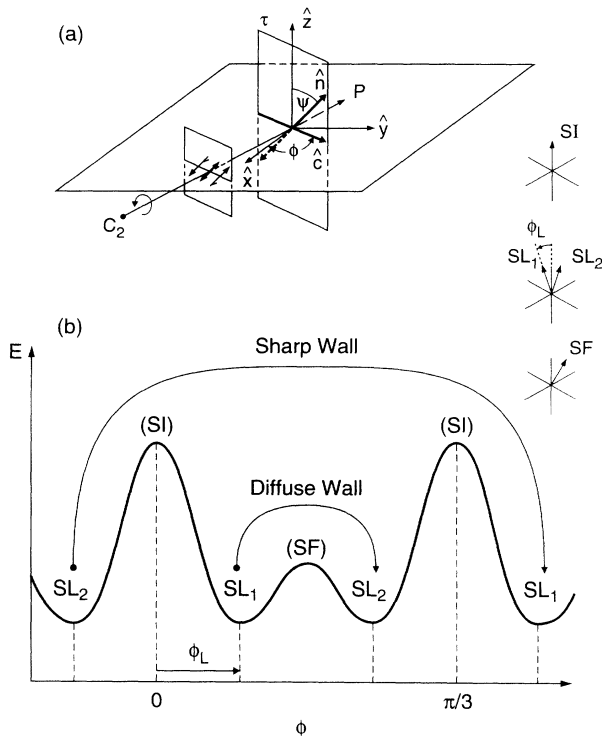


FIG. 1. Geometry and symmetry of tilted hexatic smectic films. The layer normal  $\hat{z}$  and the director  $\hat{n}$  define the molecular tilt plane  $\tau$ . The *c*-director  $\hat{c}(x, y)$ , representing the projection of  $\hat{n}$  onto the layer plane with a direction (“head”) specified, is also in the tilt plane and has an azimuthal orientation  $\phi(x, y)$ . For a phase of chiral molecules, sketched in the separate plane shown parallel to  $\tau$ , the only symmetry element present is a *C*<sub>2</sub> rotation axis perpendicular to  $\tau$ ; the associated polarization vector **P** is also indicated. For a phase of nonchiral SC molecules, there is also reflection symmetry  $\sigma$  with respect to the tilt plane. In the SI and SF phases, the *c* director is constrained to point, respectively, along and midway between the hexatic bond axes. The tilt plane  $\tau$  is therefore a reflection axis of the hexatic bond field and the symmetry of the phase is the same as that of the molecules. In the SL phase, however, where the *c*-director orientation is between the SI and SF positions, this is not the case, leading, under circumstances described in the text, to chiral symmetry breaking. A pair of such chiral substates, SL<sub>1</sub> and SL<sub>2</sub>, is associated with each of the six symmetry directions of the bond-angle field. Although these substates are degenerate, the height of the energy barrier to transitions between them depends on whether a bond direction is crossed or not, as indicated in (b).

The symmetry of the director,  $\hat{\mathbf{n}}$ , is fundamentally affected by the presence of an interface. In bulk LC,  $\hat{\mathbf{n}}$  has a bipolar, or up-down symmetry ( $\hat{\mathbf{n}} \equiv -\hat{\mathbf{n}}$ ) because, although an individual molecule may carry a net dipole moment enabling a distinction between its “head” and “tail,” a collection of such molecules will generally contain as many dipoles in the up as in the down orientation, so that the net dipole moment vanishes. It is thus an assembly of (at least two) molecules, rather than an individual molecule, that possesses up-down symmetry. The presence of an interface bounded by different bulk phases breaks local up-down symmetry because the molecular dipoles will generally exhibit a preference for one of the phases, and, on average, more dipoles will populate either the up or the down state. A finite net dipole moment colinear with the director  $\hat{\mathbf{n}}$  appears as a consequence, and the corresponding surface polarization  $\mathbf{P}_s$  serves as a new (vector) order parameter. Since the polarization vector associated with an individual asymmetric interface does *not* exhibit  $C_2$  symmetry with respect to rotations about the tilt plane normal, this eliminates the center of inversion there [14].

Given the convention [15] of assigning a unique direction to  $\hat{\mathbf{c}}$  by projecting an  $\hat{\mathbf{n}}$  with a component along the (fixed) *positive* layer normal, the transformation of  $\hat{\mathbf{c}}$  under a  $\pi$  rotation about  $\hat{\mathbf{x}}$  is found to be [5]

$$C_2^{[\hat{\mathbf{x}}]} \left\{ \hat{\mathbf{c}} \begin{pmatrix} x \\ y \end{pmatrix} \right\} = \hat{\mathbf{c}} \begin{pmatrix} x \\ -y \end{pmatrix} = \begin{pmatrix} -c_x \\ c_y \end{pmatrix}$$

while the transformation under reflection through the  $\hat{\mathbf{y}}\text{-}\hat{\mathbf{z}}$  plane is described by

$$\sigma^{[\hat{\mathbf{y}}, \hat{\mathbf{z}}]} \left\{ \hat{\mathbf{c}} \begin{pmatrix} x \\ y \end{pmatrix} \right\} = \hat{\mathbf{c}} \begin{pmatrix} -x \\ y \end{pmatrix} = \begin{pmatrix} -c_x \\ c_y \end{pmatrix},$$

as illustrated in Fig. 2.

These expressions allow us to evaluate the transformations of terms linear in  $\nabla \cdot \hat{\mathbf{c}}$  and  $\nabla \times \hat{\mathbf{c}}$ , which would correspond to possible splay and bend terms in a Landau-Ginzberg free energy functional for the films of interest. Given that  $\partial_x \mapsto \partial_x$  and  $\partial_y \mapsto -\partial_y$  under  $C_2^{[\hat{\mathbf{x}}]}$ , one finds that only  $\partial \times \hat{\mathbf{c}}$  is invariant under the  $C_2$  rotation about the tilt plane normal [5]. In contrast, reflection through the tilt plane,  $\sigma^{[\hat{\mathbf{y}}, \hat{\mathbf{z}}]}$ , yields  $\partial_x \mapsto -\partial_x$  and  $\partial_y \mapsto \partial_y$ , leaving only  $\nabla \cdot \hat{\mathbf{c}}$  invariant.

The first scenario is relevant to assemblies of chiral molecules,  $\nabla \times \hat{\mathbf{c}}$  in that case corresponding to  $\nabla \cdot \mathbf{P}$ , since  $\mathbf{P}$  is oriented normal to  $\hat{\mathbf{c}}$  [Fig. 1(a)]. The second scenario, admitting terms linear in  $\nabla \cdot \hat{\mathbf{c}}$ , is the one pertinent to an assembly of nonchiral molecules near an asymmetric interface. Such an assembly is thus, in terms of the symmetry of the  $c$ -director order parameter, formally equivalent to films of chiral material. Theories for the latter may thus be transcribed to apply to the former case by exchanging  $\hat{\mathbf{c}}$  and  $\mathbf{P}$  as the order parameter.

Since it is the mirror plane which specifically excludes terms linear in  $\nabla \times \hat{\mathbf{c}}$  for nonchiral molecules, these are allowed when reflection symmetry about the tilt plane is broken, such as takes place in the case of a chiral SL phase as we will see below.

As a consequence of the linear  $c$ -director splay, there

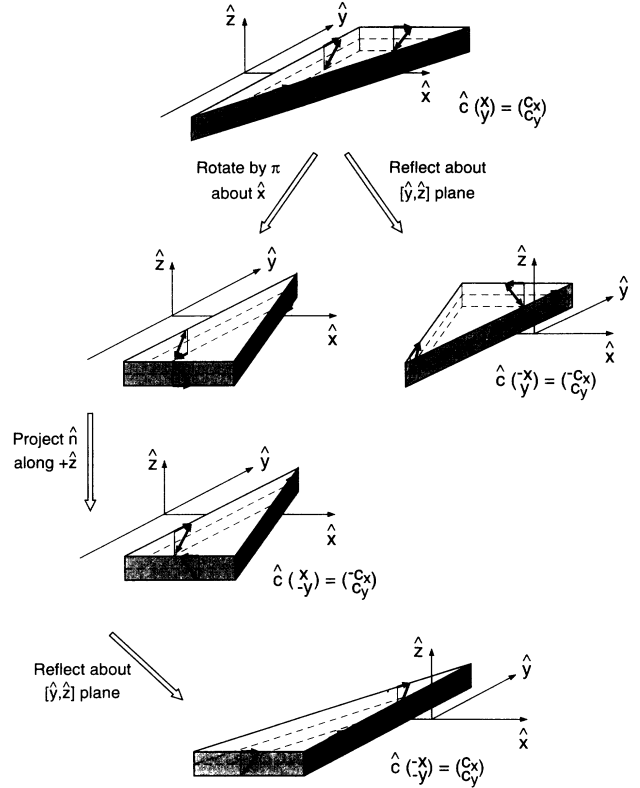


FIG. 2. Symmetry operations of tilted smectic films. This figure illustrates the transformation of  $\hat{\mathbf{c}}$  under the  $C_2$  and  $\sigma$  symmetry operations shown in Fig. 1. The  $c$  director is by convention the layer-plane projection of the director  $\hat{\mathbf{n}}$  chosen to have a component along the positive layer normal  $+\hat{\mathbf{z}}$ .

are at least two cases, as pointed out by Hinshaw and Petschek [6], in which one could expect the spontaneous formation of periodic  $c$ -director *splay* domains in films of nonchiral material.

The first case concerns films entirely in phase and bounded above and below by the same medium, such as a SC film in air. By allowing the director orientations at the two film surfaces to be independent of each other, thereby breaking the up-down symmetry of the film, Meyer and Pershan were able to construct an elastic free energy which was minimized by the formation of periodic surface splay domains separated by disclination sheets in the director field. The disclination sheets only penetrate a limited depth into the film interior in their model and are out of register with those originating at the other film surface, the idea being that when the surfaces are far enough apart the surface ordering can overcome the strong interlayer coupling of the director orientation field. Such structures were proposed to explain the existence of the periodic surface domains observed along the very thick edges of freely suspended SC films [14] and at the free surface of nematics near the SC transition [16].

Second, a tilted phase film suspended between two *different* fluids clearly has no such requirement of up-down symmetry and can therefore spontaneously form uniform  $c$ -director splay domains. This very geometry is found in monomolecular amphiphilic films adsorbed at the air-water interface (Langmuir films), where polar ordering is

a consequence of the preferential “heads down” orientation of the molecules adsorbed on the water.

The full  $S_2$  symmetry of the bulk nonchiral films can be restored by coupling two asymmetric interfaces in such a way that their respective net dipole moments cancel. This requires antiparallel orientation of the molecules near the two interfaces considered, so that  $\mathbf{P}(L/2) = -\mathbf{P}(-L/2)$  for a layer of thickness  $L$ . Such a cancellation would be expected in free-standing films of nonchiral molecules sufficiently thin to permit the coupling of the individual surface polarizations.

### B. Smectic $L$ as a chiral phase

In determining the full symmetry of the tilted hexatic phases, we need to consider both the molecular symmetry and that of the associated bond lattice. The  $\sigma$  plane of tilted nonchiral molecules remains a symmetry element of the SI and SF, since the molecular tilt plane is always coincident with a reflection plane of the bond lattice in these phases. In the SL phase, on the other hand, the  $c$  director is *not* along a symmetry direction of the bond field and the phase has *no* plane of mirror symmetry normal to the layers. When, in addition, reflections through the layer plane (and hence the  $C_2$  rotation normal to the tilt plane) are prohibited by an interface, the phase has no improper axis of symmetry and the symmetry between the substates  $SL_1$  and  $SL_2$ , which are offset left and right of the bond direction by the angle  $\phi_L$ , is broken. In other words, the SL phase is then *chiral*, with the energetically equivalent  $SL_1$  and  $SL_2$  corresponding to the enantiomeric substates of the phase [see Fig. 1(a)]. As mentioned in Sec. I, a pair of such chiral substates is associated with each of the six symmetry directions of the bond-angle field. Transitions between these states which occur in the same sense on the tilt cone,  $SL_1 \rightarrow SL_2$  and  $SL_2 \rightarrow SL_1$ , generally require different energies, as sketched in Fig. 1(b).

The chiral nature of the “surface SL” phase is therefore of essentially different origin from that associated with a phase of intrinsically chiral *molecules*, which has no improper rotation axis in any tilted phase.

According to Selinger and Nelson, the chiral nature of the surface SL phase leads to the appearance of domains of alternating SL chirality even in films of *nonchiral* LC. In principle, both periodic bend- and splay-type domains can be preferred over the uniform state and can be accounted for by a continuum elastic theory [17,18]. This theory treats the offset angle between the  $c$ -director and bond fields ( $\theta - \phi$ ), which is the same as  $\phi_L$  except in domain walls, as a chiral order parameter. Modulated states are found by minimizing a free energy functional in which this order parameter is coupled to terms linear in  $\nabla \cdot \hat{\mathbf{c}}$  or  $\nabla \times \hat{\mathbf{c}}$ . The resultant domains can either be manifested as linear stripes or as a checkerboard pattern. Theory also predicts the evolution of preexisting six-armed SI or SF star defects into characteristic 12-armed SL “petal” structures [19].

In fact, a stable stripe phase has recently been discovered by Knobler and co-workers in Langmuir monolay-

ers, in the tilted “liquid-condensed” phase of several fatty acids [20,21]. Polarized fluorescence microscopy measurements revealed a splay rotation of the  $c$ -director orientation across each stripe [22]. The additional observation of chiral star defects with curved arms led Selinger to propose that this texture was in fact a manifestation of *smectic-L* symmetry, the SL being the only intrinsically chiral monolayer phase [17].

Apart from these monolayer observations, the SL phase has so far been positively identified only in a single lyotropic system [specifically, in thick, hydrated, multilayer films of the phospholipid DMPC (dimyristoyl phosphatidyl choline)], on the basis of x-ray scattering experiments [9]. Chiral symmetry breaking has also recently been reported in scattering experiments on monolayers of the related phospholipid DMPE (dimyristoyl phosphatidyl ethanolamine) on water [23].

### III. EXPERIMENTAL METHOD

Freely suspended films both 3 mm and 6 mm in diameter were drawn in the smectic- $C$  phase using apertures (either of machined brass or made from glass coverslips) mounted inside a temperature-controlled hotstage [24]. Both round and rectangular apertures yielded the same basic phenomenology.

Images were recorded using depolarized reflection microscopy. The smectic layers spontaneously orient parallel to the film plane [10,25] and the film is illuminated by near-normal, polarized white light. In general, if the incident polarization is not in the molecular tilt plane, the optical anisotropy of the LC molecules causes the polarization vector of the reflected light to be rotated toward  $\hat{\mathbf{c}}$ . Spatial variations of perceived intensity can therefore be related to azimuthal orientation, enabling a systematic determination of the director field  $\hat{\mathbf{c}}(x, y)$ . Optical diffraction patterns were obtained in transmission by imaging incident laser light ( $\lambda = 543$  nm,  $I_0 \sim 5$  mW) in the back-focal plane of a 20 $\times$  objective with the aid of a Bertrand lens.

Film thickness was estimated from the film’s interference color [26] or, in the case of some very thin films, measured by their reflectivity of laser light [27].

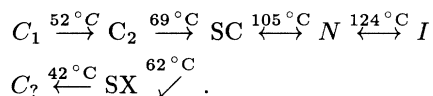
Several LC materials were investigated, including the terphenyl ester FTE1 [28] and the well-known Schiff’s base homologs 7O.4, 5O.7, and 7O.7 [29]. Freely suspended films of all of these compounds exhibit the SC and some tilted hexatic phases and they *all* show similar modulated textures. Because of its superior chemical stability, however, the terphenyl compound was found to be better suited to extended experimentation than the hydrolysis-prone Schiff’s base materials [30,31].

FTE1 is a fluorine-substituted terphenyl ester synthesized by a cross-coupling reaction of a biphenyl and a phenyl unit catalyzed by a palladium complex [28]. The product was purified by means of silica-gel column chromatography using chloroform-alkane mixtures [such as chloroform-heptane (7:3)] as a solvent. This was followed by a recrystallization in ethanol, the final purity being estimated as at least 95%. Differential scanning calorimetry (DSC) reveals several bulk phase transitions

and the LC phases can be partially identified with the aid of optical microscopy. Figure 3 shows DSC data for both heating and cooling. The transition enthalpies are proportional to the integrated peak intensities of these scans.

The heating curve shows at least four endothermic phase transitions. Each of the first two peaks exhibits an additional shoulder on the low-temperature side of the maximum, which implies that there are probably two phase transitions taking place in a very narrow temperature range here. Textural observations of an FTE1 sample melted between glass slides and viewed in polarized light allow the assignment of the biggest peak in the heating curve (at 69 °C) to the crystal-SC transition, the latter phase showing typical SC schlieren and fan textures. The next peak (at 105 °C) corresponds essentially to a SC-nematic transition: a very narrow intervening smectic-A (SA) phase can be seen under the microscope but is not resolved in the DSC. Finally, we note that the heating curve also shows a broad exothermic peak (dipping below the baseline) at low temperatures, corresponding to a transition from a supercooled metastable phase to a stable crystalline phase.

These observations imply a phase sequence on heating which includes at least the following bulk transitions:



The lower-temperature peaks in the cooling curve are shifted and of different magnitude from those observed on heating. Supercooling of crystalline phases is common in liquid crystals and makes the interpretation of these data difficult. However, the relatively small transition enthalpy of the peak at 62 °C suggests the possible existence of a monotropic smectic phase, denoted SX in the diagram below.

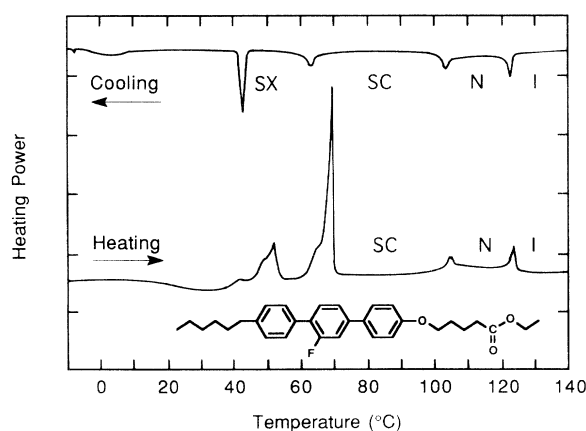


FIG. 3. DSC curves for the compound FTE1. The data are for an 8 mg sample and were obtained on a Perkin Elmer DSC 2c at a scan rate of 5 °C/min. The second heating and cooling runs are shown. The tick spacing on the vertical axis corresponds to 0.5 mcal/sec. Only those phases whose identification is unambiguous are labeled.

The bulk phase sequence can be used as a starting point for understanding the phase behavior of FTE1 in freely suspended films. As with other LC materials, however, the phase sequence in thin films shows distinct differences from the bulk. For example, no SA phase is seen in thin films of FTE1, this phase presumably being suppressed in favor of the SC. The SC phase in films has a similar range to that of the bulk phase but the bounding transition temperatures are elevated about 10 °C above the bulk values. In addition, tilted hexatic phases appear below the SC which exhibit the modulated textures that are the subject of this paper.

Unless specifically stated otherwise, all photomicrographs are of films of FTE1, viewed in reflection with slightly decrossed polarizers.

#### IV. EVOLUTION OF TEXTURES WITH TEMPERATURE

We have made careful studies of the textures of films of uniform thickness, as well as of films containing islands, while cooling from the SC to the underlying hexatic phases.

##### A. Linear modulations in uniform films

For films thicker than about ten layers, we repeatedly see the following general sequence of textural changes.

##### 1. Smectic-C phase

The texture well in the SC phase is characterized by rapid, large-scale fluctuations in the director field: broad, fluctuating extinction brushes, sometimes emanating from point singularities in  $\hat{c}(x, y)$ , represent typical features of this phase [10]. Frequently, SC films within a few degrees of the lower SC phase boundary also contain thin, curvilinear defects, from a few to several hundred micrometers in length, which separate regions of different director orientation. These often nucleate at the edges of the film or at layer steps, and either exist as isolated segments only a few micrometers in length or may generate curved sidearms forming large, complex treelike structures. When densely packed, they resemble the fingerprint textures of cholesteric LC [32]. These director field defects are found in both chiral and nonchiral materials and have been compared by Pang *et al.* [33] to the strings predicted for XY-like systems [34].

##### 2. SC-hexatic transition

Upon cooling to just ( $\lesssim 1^\circ\text{C}$ ) above the hexatic transition (about 81 °C in FTE1), there is a dramatic increase in the magnitude of the director fluctuations, likened by Amador *et al.* to critical opalescence [35]. Simultaneously, we observe transient, anisotropic correlation regions, which are typically about 100  $\mu\text{m}$  in extent, devel-

oping perpendicular to  $\hat{c}(x, y)$ , an effect also previously seen in a different Schiff's base material at the SC-SI transition [36]. With further cooling, director fluctuations are reduced again, leaving a large-scale, frozen texture of oblong domains (bâtonnets) that resembles the classical focal-conic fan texture of smectic LC prepared between glass plates [37]. In general, a focal-conic texture is evidence of an underlying periodic structure. In the present case, this could well be the onset of the line phase described below, but since the wavelength is too small to resolve optically we cannot be certain of this.

Concomitantly, the formerly broad extinction brushes essentially collapse on themselves [Fig. 4(a)], signaling the evolution of transient (SC) correlation regions into permanent domains (grains) of rather uniform director orientation separated by distinct walls (grain boundaries). These walls are presumably generated as a response of the growing hexatic bond-orientational ordering field to the director topology inherited from the SC

phase, in a manner similar to that leading to star defects in some SI films [12]. In the material 7O.7 these phenomena occur very near 78 °C, the temperature at which x-ray measurements reveal that the two outermost layers of the film undergo a transition into the SI phase, the film interior remaining SC [26].

### 3. Lines

After minimal further cooling, the film in many cases now displays an array of thin disclination lines, spaced 0.5–2  $\mu\text{m}$  apart. These are overlaid on the existing texture with an orientation parallel to  $\hat{c}(x, y)$  so they are most probably splay defects [38]. The director orientation between each pair of lines is initially difficult to resolve but on lowering the temperature the lines move further apart and each band is seen to have an obvious gradation from dark to bright, implying that the director

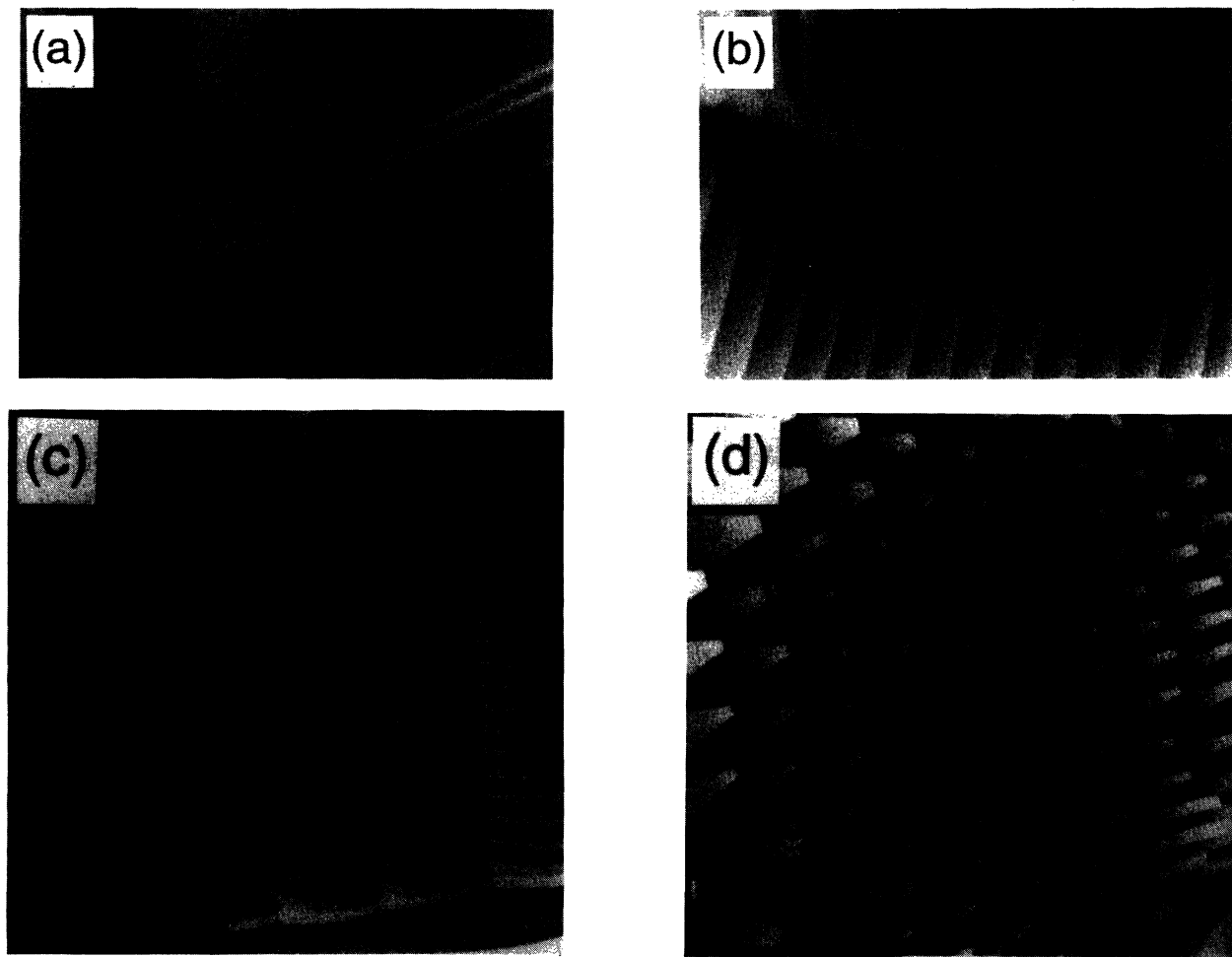


FIG. 4. Modulated textures in hexatic films. (a) Evolution of SC brushes to strings. The broad extinction brushes of the SC phase collapse to sharp strings when cooled to the hexatic phase transition ( $T \sim 80^\circ\text{C}$ ). When the film is subsequently heated, the inverse process, wall broadening, occurs. (b) Coexisting stripe and line texture in 7O.4 ( $T \sim 75^\circ\text{C}$ ). (c) Stripes near film edge, modulated by perpendicular line defects (brick wall texture). The stripes are bent into cusps at each line defect and can pass through only every second line unchanged ( $T \sim 73^\circ\text{C}$ ). (d) Honeycomb texture at low temperature ( $T \sim 65^\circ\text{C}$ ). The insets in (c) and (d) show details of the texture near bend walls. The horizontal dimension of (a) and (b) is about 250  $\mu\text{m}$ , of (c) and (d) about 130  $\mu\text{m}$ .

rotates continuously across each band [Fig. 4(b)]. That is, the line texture is composed of bands of continuous director splay, separated by splay disclinations.

#### 4. Stripes

The coarse-grained texture with superimposed disclination lines just described persists at most over a couple of degrees [39] and then transforms into a phase of parallel, uniform stripes of well-defined, temperature-dependent periodicity  $d$ , initially of the order of 2–5  $\mu\text{m}$ . The stripes form parallel to the original line texture, each splayed band typically evolving into precisely one light and one dark stripe [Fig. 4(b)]. This evolution essentially involves broadening of the lines, which either takes place homogeneously (simultaneously) everywhere on the line, or is achieved by motion of a line-broadening front traveling along the line. The director orientation appears to be *uniform* within each stripe and jumps alternately by a fixed angle  $\pm\delta\phi$  in the range  $25^\circ \lesssim |\delta\phi| \lesssim 35^\circ$  when crossing stripe boundaries, which are sharp (resolution-limited), weakly undulating walls. The original grainy domain texture frozen in from the SC phase is rapidly annealed out and is then no longer visible in the stripe phase. When the film is left to equilibrate, within a few hours the stripes form a few well-oriented, almost defect-free regions spanning the film and this texture is extremely stable, existing unchanged for many days. The resulting stripes have a well-defined periodic structure which gives rise to several orders of Bragg scattering of visible light (Fig. 5).

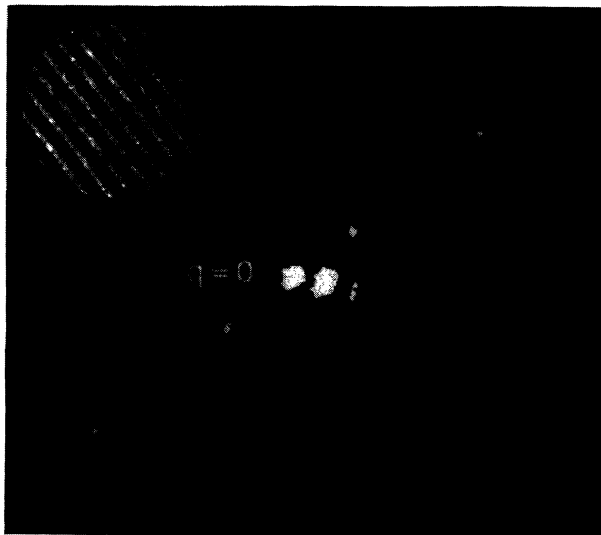


FIG. 5. Optical diffraction pattern from a striped film ( $T \sim 68^\circ\text{C}$ ). This computer-enhanced image shows the first and third order peaks as well as the central maximum. Fifth order spots were visible by eye but fell outside the imaging area of the camera. The two off-axis spots near the central maximum are stray reflections of the main beam; the even order peaks are absent. The inset shows a circular region of uniform light stripes such as were illuminated in the diffraction experiment.

The stripe period increases monotonically with decreasing temperature, as was illustrated in Ref. [8]. This broadening of the stripes is reversible provided that the temperature is changed slowly but rapid heating also leads to buckling, a response, familiar from magnetic systems, that reduces the stripe period without having to introduce new stripes [40]. An example of this is shown in Fig. 6.

We have seen no evidence (such as overlapping domains or misaligned stripes) that would indicate independent or different director orientations on the two film surfaces. The high degree of optical contrast between the stripes suggests that the director azimuth,  $\phi$ , is fairly constant through the thickness of the film [41]. Weak SC-like director fluctuations are observable in the background throughout the stripe phase, although they become less visible with decreasing temperature. Stripes occur in films with thickness ranging from about ten to at least 60 layers (i.e., with interference colors from black to green). There is *no* strong dependence of stripe width on film thickness in this range, with stripes passing continuously and apparently unchanged across steps in film thickness of the order of 15 smectic layers or more. However, in a 5.06 film only about six layers thick, *no stripes were observed* throughout the hexatic range, the film retaining instead the coarse texture of large-scale correlation regions frozen in from the SC phase. Similarly, FTE1 films with only two layers showed only the phase transitions and broad band textures normally associated with SI and SF phases in freely suspended films [12,42], and no stripes in the relevant temperature range [43].

The stripe phase persists down to about  $73^\circ\text{C}$  in 7O.7, the temperature at which the x-ray experiments show that, in addition to the surfaces, the film interior too transforms into the SI phase [26]. At this point the director fluctuations and domain wall undulations are finally quenched and the stripes slowly evolve to the broad, graded bands characteristic of many SI and SF films [12,42]. This expansion is often achieved by the expulsion of alternate stripe boundaries to the edges of the film, a process basically the reverse of the original hexatic line-stripe transition: the low-temperature banded textures are, however, much less regularly spaced than the high-temperature line array.



FIG. 6. Stripes buckling in response to rapid heating ( $T \sim 76^\circ\text{C}$ ). The horizontal dimension is about 250  $\mu\text{m}$ .

At even lower temperatures, the films often acquire a crystalline appearance and are presumably in a smectic crystal phase.

### 5. Strings and hexatic line defects

Several important additional defect structures are frequently seen in the stripe phase. Stringlike defects first appearing in the SC can persist into the stripe phase, where they are indistinguishable from line defects generated by the condensation of broad walls at the hexatic transition. Hexatic line defects are always associated with characteristic additional modulations of the basic one-dimensional stripe pattern described above.

Two limiting cases can be distinguished: line defects oriented *parallel* to the stripes are associated with a monotonic evolution of the stripe intensities normal to the stripe direction. The location of these defects is marked by an interruption of the prevailing regular alternation of dark and light stripes, and the onset of a new pair of stripe intensities; this shading then evolves over several stripe pairs back to the original two intensities.

When *perpendicular* to the stripes, as is usually the case, the line defects appear as sharp domain walls across every *other* stripe and lead to long-wavelength modulations of the director field along the stripe direction. Remarkably, they also cause the stripe orientation to be distorted locally into a cusp. An array of such defects generates a film texture resembling a brick wall [Fig. 4(c)], which evolves into a honeycomb texture [Fig. 4(d)] on further cooling.

Grain boundaries at *intermediate orientations* are accommodated by linking alternating parallel and perpendicular string segments, resulting in a rather mobile texture resembling the wandering steps seen on atomically grown surfaces [44].

We will discuss hexatic line defects and their role in determining film textures at length in Sec. VI.

### B. Circular geometries—*islands*

Lateral temperature gradients or the accumulation of surplus material while the film is being drawn can lead to the spontaneous formation of circular islands, which are uniformly thick regions where there are extra layers. These layers probably float within the film and the edge dislocations defining their perimeter serve to constrain the director field topologically and mark the boundary of the island. The well-defined geometry of such islands has allowed observations of textural transitions which are crucial to our understanding of the hexatic stripe phase.

In the SC phase, a point singularity in the director field appears spontaneously near the middle of each island because of the symmetry imposed by its circular boundary, yielding a characteristic four-brush extinction pattern when viewed between crossed polarizers. The relative rotation of these brushes when the polarizers are decrossed slightly shows that the basic orientation of the

*c* director in these islands is *circumferential* [45], i.e., the point defect forms the center of a *bend* distortion. This configuration minimizes the elastic free energy when, as expected, the Frank elastic constant for splay is greater than that for bend ( $K_S > K_B$ ) [25]. The anisotropic correlation regions that form on cooling to the SC-hexatic transition are always extended *radially* inside these islands, along the *splay* fluctuation direction.

Upon further cooling, stripes form as concentric rings and a 12-armed radial star defect appears in each island. The arms terminate at the edge of the island, are usually curved, and are often unevenly spaced. Although ten- and 14-armed defects occasionally occur, the overwhelming preference for 12 arms suggests that each arm preferentially mediates an average change of director orientation of about  $30^\circ$  ( $2\pi/12$  rad). The stripes are modulated along their length and each stripe is apparently able to pass through every other radial arm unchanged, as can be seen in Fig. 7(a). This gives each ring-shaped stripe the appearance of being azimuthally rotated half a “modulation period” ( $30^\circ$ ) relative to its neighbors. We recognize this equilibrium configuration as being the familiar brick wall pattern bent around in a circle. This implies that the wall defects crossing linear stripes [Fig. 4(c)] and the arms of the star are topologically equivalent. In addition, the fact that stripes always form concentrically in islands with central director bend defects confirms that stripes correspond fundamentally to *splay*-

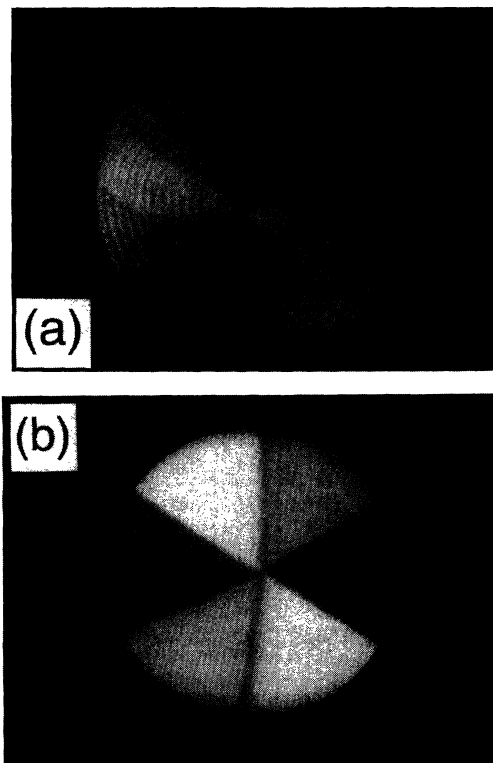


FIG. 7. Modulated hexatic textures in islands. (a) Concentric stripes modulated by a 12-armed star defect ( $T \sim 71^\circ\text{C}$ ). The horizontal dimension is about  $250\ \mu\text{m}$ . (b) Six-armed star defect at low temperature ( $T \sim 61^\circ\text{C}$ ). The surrounding film is considerably thinner and thus darker than the islands.

like modulations of the director field. Variations along the stripes are therefore *bendlike*. As we will discuss below, the specific intensity patterns displayed in the brick wall texture strongly constrain possible models of the director configuration and the assignment of symmetry to the stripe phase.

Upon further cooling, the stripe phase disappears and the 12-armed star defects evolve (reversibly) to *six-armed* stars, usually with straight arms [Fig. 7(b)]. Each arm of this new defect mediates a change of  $\Delta\phi \sim 60^\circ$  and delineates six sectors of *uniform* director orientation, as indicated in Fig. 8. The ends of the arms are anchored along the edge of the island and it is this boundary which energetically stabilizes six arms [20] rather than the five seen by Dierker *et al.* around an isolated point defect in a SI film [12]. The six-armed stars are reminiscent of similar defects seen in bulk smectic-*F* droplets surrounded by the isotropic LC phase [46] and, more recently, inside hexagonal domains in tilted hexatic Langmuir monolayers [20].

The transformation from six- to 12-armed stars begins with a destabilization of the linear arms which causes them to expand at intervals along their length into smooth, rounded domains of different sizes. These regions expand until they make contact with their neighbors and, on further heating, transform into regular circumferential stripe domains of the type seen in 12-armed stars. A typical intermediate state is shown in Fig. 9.

This concludes our initial description of the experimental observations.

## V. PROPOSED MODEL

We now present a model of the stripe textures in our films, mindful of the possible mechanisms for the formation of modulated textures outlined in Sec. II.

Specifically, we propose that the stripes represent a

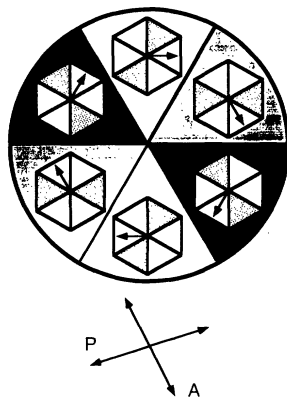


FIG. 8. Director field in a six-armed star. The *c* director is uniform in each sector and the six orientations shown here correspond to equilibrium azimuths of the SF phase. The polarizer and analyzer are decrossed, yielding three distinct reflection intensities. The bond orientation lattice rotates through  $|\Delta\theta| = 120^\circ$  in each arm, the shading of two segments of the lattice enabling visualization of its absolute orientation.



FIG. 9. Evolution of six- to 12-armed stars on heating ( $T \sim 64^\circ\text{C}$ ). The straight arms of the original six-armed star have destabilized and are no longer recognizable. On further heating, the irregular bulging domains seen in this picture extend circumferentially and reorganize into regular stripes modulated by a 12-armed star. The diameter of the larger island is about  $170\ \mu\text{m}$ .

modulated phase resulting from breaking of local (up-down) reflection symmetry analogous to that in Langmuir films, combined with the onset of hexatic bond-orientational order. This symmetry breaking is a consequence of the incomplete wetting of the air-SC interface by a newly appearing surface hexatic phase on cooling from the SC, a phenomenon explicitly demonstrated by the Pershan group in x-ray scattering experiments on the materials 7O.7 and 5O.6 [35,26]. Films up to a thickness of about 35 layers were found in their experiments to exhibit an intriguing two-step SC-SI transition: First, the two surface layers “freeze” into the SI, the interior remaining essentially SC but probably taking on some local hexatic ordering induced by the surface layer [35]. In this intermediate phase, denoted “SI/SC”, molecules close to the surface are considerably more tilted than those in the interior [47]. Upon further reduction of the temperature, a continuous increase of the surface hexatic order is eventually terminated by the abrupt (first order) condensation of the entire film interior into the SI phase. This is followed at even lower temperatures by a homogeneous transition of the entire film to the SF phase.

Significantly, the range of temperatures over which we see stripes in 7O.7 corresponds very closely to the temperature range of the so-called SI/SC phase. Since the original x-ray phase identification was based primarily on radial scans through an azimuthally powder-averaged scattering pattern, there is some uncertainty that the surface phase really is SI [48]. The experiments leave no doubt, however, that the surfaces are hexatic and the film interior SC-like at these temperatures.

In SI and SF films, the observed jump in director orientation across domain walls or star arms is typically found to be to  $\Delta\phi = 60^\circ$ , corresponding to the angle between neighboring hexatic bond orientation axes [12]. Although such simple splay walls as are allowed by SI symmetry [17] may explain the higher-temperature line texture of our films, a director field with SI (or SF) symmetry *cannot* account for the characteristic intensity dis-

tributions of linear and circular stripe patterns decorated by transverse bend walls observed at lower temperatures. In particular, the typical magnitude ( $25^\circ \lesssim |\Delta\phi| \lesssim 35^\circ$ ) of the observed jump in director orientation from stripe to stripe is fundamentally incompatible with the pseudo sixfold symmetry of the bond-angle field to which  $\hat{c}$  is locked in the SI (or SF) phase.

However, the existence in the SL phase of 12 energetically equivalent states and *two* different wall energies (the height of the energy barrier between  $SL_1$  and  $SL_2$  depending on whether there is an intervening bond direction or not) allows the construction of a model that is consistent with all of our observations, namely, that *the stripes correspond to alternating smectic-L domains,  $SL_1$  and  $SL_2$* . SL symmetry would not only explain the director orientations measured in the stripe phase, but is also consistent with the specific hexatic textural changes with temperature observed in our films, as we shall see below.

In general, hexatic grain boundaries form perpendicular to gradients in  $\phi$ . They locally relieve the strain between the director  $\phi$  and hexatic bond lattice  $\theta$  orientations by allowing a phase slip in the offset angle ( $\theta - \phi$ ). In our model of the stripe phase, each transverse domain wall (or radial arm) and each stripe boundary mediates a change in SL *chirality*. This proposed structure is a two-dimensional variant of one-dimensional SL stripe structures proposed by Selinger [17] to explain the patterns observed in Langmuir films.

In the brick wall pattern of Figs. 4(c) and 10(a) the stripes are crossed, nearly at right angles, by a second set of walls. With the identification of the stripes as  $SL_1$ ,  $SL_2$  domains separated by splay walls, it is natural to suppose that the second set of lines be bend walls. Figure 10(b) shows a composite splay wall–“stripes” bend wall–“lines” structure in which the bend walls merely switch the chirality of the stripes. This kind of two-dimensionally modulated structure, where the director is wobbling between symmetric positions about the local stripe direction in a periodic fashion, is consistent with the basic optical observations.

Given this fundamental structure for walls and stripes, though, several characteristic geometrical features of the brick wall pattern still need to be explained. For example, for a given bend wall, the  $c$ -director jump is sharp only in every *other* stripe, being diffuse in the intermediate stripes; and the “sharp” and “diffuse” bend walls also alternate *along* the stripes, which is what directly gives rise to the brick wall pattern of overlapping tiles. In the model of Fig. 10(b), all of the bend walls are equivalent, the director jumps simply being of opposite sign. Thus this model would predict uniformly sharp bend walls at every stripe and a symmetry not exhibited in the brick wall pattern.

That there are ways of producing nonequivalent jumps of  $\hat{c}$  is evident from the energy vs  $c$ -director orientation diagram  $E(\phi)$  in Fig. 1(b). Here we see that there are several energetically different possible paths by which  $\hat{c}$  can go from  $SL_1$  to  $SL_2$ . In the model of Fig. 10(b), all of the jumps, whether parallel or transverse to the stripes, are through the SI orientation [i.e.,  $(SL_1 \rightarrow SI \rightarrow SL_2)$

and  $(SL_2 \rightarrow SI \rightarrow SL_1)$ ] and are thus equivalent, as noted above. The next simplest scenario is to assume that the jump sequence along a stripe is  $(SL_1 \rightarrow SI \rightarrow SL_2)$  then  $(SL_2 \rightarrow SF \rightarrow SL_1)$ , the  $c$  director passing alternately

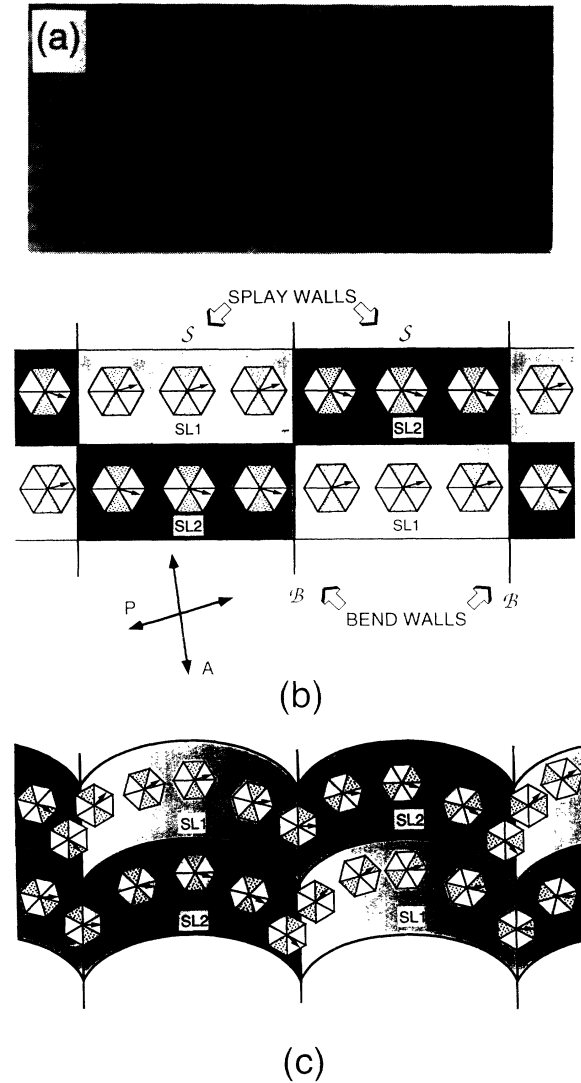


FIG. 10. Brick wall texture. (a) Array of line defects in the form of bend walls, decorating a stripe phase in the linear geometry and leading to the appearance of an intensity pattern in the form of a brick wall. The stripe period is approximately  $12 \mu\text{m}$ . (b) Naive proposed smectic-L bond and director fields for the brick wall texture in (a). Each lateral stripe boundary represents a splay wall which also mediates a change in SL chirality. Additional transverse line defects in the form of bend walls also mediate a change in SL chirality. The director field is nonuniform, bending along the stripes to give the characteristic observed intensities. (c) Refined version of the model in (b), in which a steady rotation of the bond field along the stripe direction results in an average  $\pi/3$  phase slip between bond and director fields for each crossing of a bend wall. The shaded hexagon segments labeling an arbitrary (but definite) symmetry direction of the hexatic lattice make the bond field rotation plain. The stripes curve to follow the lattice orientation, leading to the formation of cusps at the bend walls.

through the SI and the SF orientation at successive bend walls. This scenario would require a  $\pi/6 \equiv 30^\circ$  rotation of the hexatic lattice as one moves from line to line along the stripes, with the nearest-neighbor rows (SI tilt direction) parallel to the stripes at one line crossing and next-nearest-neighbor rows (SF tilt direction) parallel to the stripes at the next. There is no fundamental problem with this kind of rotation since the lattice is hexatic. However, this scenario also requires a  $\pi/6$  rotation of the lattice as one moves along a line in the *transverse* direction (i.e., from stripe center to stripe center). This kind of rotation is not seen experimentally.

The next possibility is to have an average  $\pi/3 \equiv 60^\circ$  lattice rotation along the stripes between each pair of lines. This structure, shown in Fig. 10(c), is consistent with the features found in the optical observations. In this model the *c*-director jump across the bend walls alternates between the two indicated in Fig. 1(b), namely,  $(SL_1 \rightarrow SF \rightarrow SL_2)$   $(SL_2 \rightarrow SL_1 \rightarrow SF \rightarrow SL_2 \rightarrow SL_1)$ . The lattice has the SF bond oriented along the mean stripe orientation at every line (bend wall) and the lattice orientation is the same from stripe to stripe.

In summary, we are proposing that the brick wall pattern is a result of a continuous rotation of the hexatic lattice relative to the mean *c*-director orientation. The brick wall texture corresponds to a regular checkerboard arrangement of oblong  $SL_1$  and  $SL_2$  domains, with the non-uniform optical appearance of the individual domains resulting from director bend along the stripes. This director configuration is qualitatively consistent with the observed intensity distributions and explicitly realizes the requisite jumps in chirality of the surface SL phase. The spontaneous domain structures induced in the hexatic surface layers would be propagated elastically through the SC film interior. We note that neighboring splay walls have alternating up-down symmetry, so that each wall is associated with a polar axis along the film normal.

This model leads directly to the interpretation of the 12-armed star defect of Fig. 7(a) as being the brick wall pattern bent about a defect core at the center of the island. The net strength of the *c*-director disclination is  $s = +1$  (since  $|\Delta\phi| = 2\pi$ ), and that of the hexatic lattice vortex  $v = -12$  (since  $|\Delta\theta| = 4\pi$ ). We have already noted that there is a temperature-mediated, reversible transformation between this structure and that of the six-armed star (see Fig. 9). The mechanism appears to be similar to one proposed by Selinger and Nelson [19] in which SL domains collapse onto the six domain walls of a SF star on cooling, and reappear on heating.

In contrast to the modulated stripe segments of the 12-armed SL structure, each sector of the six-armed SF star has a uniform *c*-director orientation. If lattice vorticity within the island is conserved during the transformation from 12 to six arms, then each SF arm must mediate a lattice rotation of  $|\Delta\theta| = 2\pi/3 \equiv 120^\circ$ , in the opposite direction to the *c*-director rotation across the arm. Dierker *et al.* proposed a structure for their five-armed SI star defect [12] with director disclination strength  $s = +1$  and a lattice vorticity  $v = +6$  (i.e.,  $\hat{c}$  and the bond field rotate in the same sense, both through  $2\pi$ ). Although the bond-director field shown in Fig. 8 looks like a straightforward

modification of the Dierker model (and indeed would be optically indistinguishable from a six-armed defect structure with lattice vorticity  $v = +6$ ), it is essentially different in that the lattice rotation in each arm is twice as big in our model, and in the opposite direction.

## VI. LINE DEFECTS

The model introduced in the preceding section for the conformations of director and bond-angle fields in the stripe phase enables us to proceed to a closer investigation of the general nature of line defects and their interaction with the stripe pattern. Line defects crossing stripes, which we have identified as director bend walls, have already been encountered in Sec. IV, both as transverse walls in the linear geometry [Figs. 4(c) and 10(a)] and as radial arms in the circular geometry of islands [Fig. 7(a)]. As can be seen in Fig. 4(c), bend lines can apparently simply end. To show that this is an illusion, we need to examine the topology of the stripe domain-bend wall intersections.

Specifically, let us consider the topological consequences of the broken chiral symmetry characteristic of the SL phase, as envisioned in the models of Fig. 10. Here, splay walls separating successive stripes, as well as bend walls in the form of transverse line defects, mediate a change in chirality. As Fig. 11(a) indicates, a closed

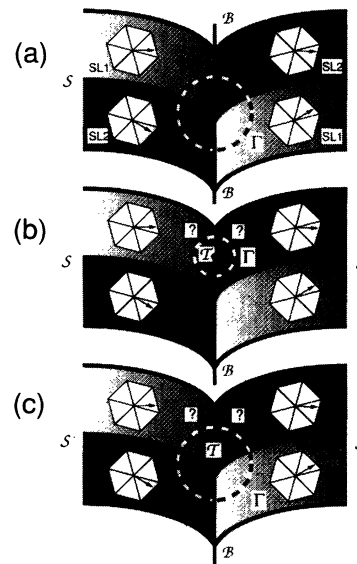


FIG. 11. Chiral topology of line defects in the stripe phase. (a) Details of bond and director fields, constructed for the surface of a SL film in accordance with the model of Fig. 10(b), at the intersection of a splay wall  $\mathcal{S}$  and a perpendicular bend wall  $\mathcal{B}$ . The intersection is characterized by a downward cusp in the stripe profile. Also shown is a contour,  $\Gamma$ , enclosing the intersection point. (b) and (c) illustrate arguments, given in the text, eliminating, respectively, the possibility of terminating a bend wall  $\mathcal{B}$ , either in the interior of a stripe, or at its intersection with a splay wall  $\mathcal{S}$ . The consequent ambiguity in the assignment of a chiral state near the hypothetical terminal point  $\mathcal{T}$  is indicated in both cases.

contour,  $\Gamma$ , about any splay wall-bend wall intersection point traverses at least two splay walls and two bend walls, or more generally an even number of each. This is a necessary condition to ensure that there is no enclosed topological charge and to avoid ambiguity in the assignment of a unique chiral state at any given position. As Figs. 11(b) and 11(c) illustrate, termination of a transverse line defect leads to a violation of this condition and must therefore be forbidden on topological grounds. This difficulty persists regardless of whether the terminal point  $\mathcal{T}$  is chosen to lie in the interior of a stripe [as in Fig. 11(b)] or on a stripe-stripe boundary [as in Fig. 11(c)]. We note that the scenario (b) is the analog of the configuration proposed for each terminus of the radial disclination lines of five-armed star defects in the SI phase [12]. While the symmetry of the SI phase permits the termination of a disclination line in a point (which consequently carries a net topological charge [12]), lowering of the symmetry to SL specifically eliminates this possibility. That is, *line defects in a chiral SL phase cannot end in a point*. Conversely, the absence of such terminal points in a hexatic phase may then be interpreted as evidence of broken chiral symmetry.

This conclusion provides the basis for our interpretation of the topology characterizing the *apparent* termination of bend walls, or transverse line defects, within a stripe pattern; examples of this are visible in Fig. 1(a) of Ref. [8] and can be seen more clearly in Fig. 12(a). The sketch in Fig. 12(b) shows a model of this situation in which the bend wall  $\mathcal{B}$  does not in fact terminate at the point  $\mathcal{T}$ , but emerges as an additional stripe-stripe (splay) domain wall  $\mathcal{S}'$ . The result of this conversion of a bend into a splay wall is the appearance of an additional semi-infinite stripe, i.e., the creation of a dislocation in the stripe pattern. The particular array of dislocations visible in Fig. 12(a) appears to facilitate an overall re-orientation of the pattern imposed by the curved film boundary.

This transformation of a bend wall into a splay wall is readily generalized to the interconversion of transverse and longitudinal line defects, which is an obvious mechanism for avoiding the termination of line defects in points. Figure 13 demonstrates that this interconversion is indeed observed: it facilitates changes in direction of line defects relative to the prevailing stripe orientation and provides the necessary ingredient for creating closed loops of line defects. A crucial observation, illustrated by this figure, is that line defects do in fact either form loops, or terminate at film boundaries or other inhomogeneities disrupting the entire stripe pattern, as in the example of Fig. 10(a). This topological characteristic of line defects in a SL is analogous to that of dislocations in three dimensions [49].

A closer inspection of the pattern in Fig. 13 reveals several additional features associated with line defects in the SL phase.

A first observation concerns the cusps formed by stripes crossing a loop: these adopt *opposite* orientations on entering and leaving, as may also be seen in Fig. 14(a). This is in essential contrast to the situation encountered with arrays of transverse line defects in the

linear geometry of Fig. 10(a): there, each stripe is distorted into a sequence of arcs, forming cusps of *identical* orientation at intersections with successive bend walls. The model of Fig. 10(c) in fact suggests an intimate connection between the orientation of the cusps and that of the bond-angle field—namely, that the stripe domain walls prefer to lie along the nearest-neighbor (SI) bond direction—that gives rise to the characteristic intensity modulations of the regular brick wall pattern. Examination of the patterns in Figs. 13 and 14(a) makes clear that the intensity modulations exhibited by stripe domains intersecting a loop do *not* conform to the brick wall pattern. For example, the set of stripes which enters a loop without experiencing a discontinuity in intensity also exits from the loop without intensity change, retaining a gray color in the rendition of Fig. 14(b). The adjacent set of stripes, on the other hand, exhibits two successive discontinuities, white→black and black→white.

We conclude from this observation that the topological transformation induced in a stripe when entering the loop is reversed when leaving the loop. As the model

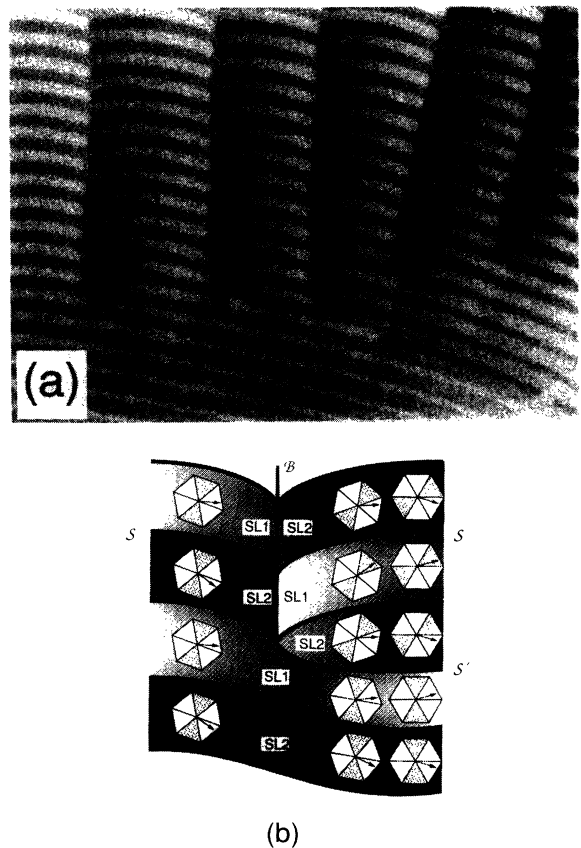


FIG. 12. Stripe dislocations terminating a bend wall texture. (a) Enlarged view of the apparent end points of the array of transverse line defects shown in Fig. 4(c). A dislocation in the stripe pattern is associated with each of the apparent terminal points. (b) Director-bond field model of the apparent terminal point of a transverse line defect  $\mathcal{B}$ , derived from that of Fig. 10(b). The model illustrates that the conversion of  $\mathcal{B}$  into an additional, distinct splay wall  $\mathcal{S}'$  requires the introduction of an edge dislocation in the stripe pattern.



FIG. 13. Curved line defects. The photograph shows a stripe pattern permeated by an array of line defects emerging from the edge of the film (part of the filmholder is visible in the lower left portion of the image). Note that the cusps associated with successive defects adopt identical orientation (pointing upward). What are initially transverse line defects convert into longitudinal defects via “faceted” curved segments. A portion of a loop is visible in the lower right of the image. Details of the intensity modulations and cusp orientations are discussed in the text. The horizontal dimension of the field of view is approximately  $180 \mu\text{m}$ .

of Fig. 14(b) illustrates, this means that no topological constraint exists to prevent the removal of pairs of stripe segments interior to the loop. The fact that the contours  $\Gamma_-$  and  $\Gamma_+$  shown in Fig. 14(c), which enclose, respectively, the two intersection points  $\mathcal{K}_-$  and  $\mathcal{K}_+$ , must be followed in *opposite* directions to realize the same sequence of stripe colors, is an expression of the opposing chiralities associated with these two intersection points. According to this model, loops are topologically unstable: we do in fact observe that they contract and annihilate in the course of annealing of stripe patterns, as illustrated in Fig. 14(a). As a result, equilibrated stripe patterns do not contain loops. These considerations imply that arrays of successive bend walls in the brick wall pattern decorated by cusps of *identical* orientation can only be removed if they are part of complete loops. If pinning at the sample boundary intervenes, as in Fig. 13, arrays of line defects of equal chirality are stable.

A prerequisite for loop formation, or indeed for any change in orientation of a line defect, is the transformation of transverse to longitudinal line defects and vice versa. In fact, our observations suggest that line defects are apparently restricted to two distinct orientation states, namely, transverse and longitudinal with respect to the prevailing stripe orientation, as illustrated in Figs. 13 and 14. Such a restriction, limiting turns to right angles, would be analogous to that restricting steps on certain crystal surfaces to the directions consistent with

the discrete symmetry of the underlying lattice [44].

We have already seen examples of the conversion of a transverse (bend) wall  $\mathcal{B}$  into a longitudinal (splay) wall  $\mathcal{S}'$ , where the conversion was accompanied by the insertion of an extra, semi-infinite stripe into the pattern in Figs. 4(c) and 12(a). In the apparently more common situation typified by Fig. 13, this creation of stripe dislocations is not observed. That is, the longitudinal segment emerging from the transverse portion of the line defect and assuming the form of an extra splay wall is not directly visible. However, the foregoing topological argument prohibiting the termination of line defects in a SL stripe pattern forces the conclusion that this extra splay wall segment must in fact be present. The intensity pattern characterizing “jagged” line defects, which shows both the usual longitudinal modulations in the stripe intensity associated with bend walls (as in Fig. 10), as well as new transverse modulations illustrated in Fig. 15(a), is therefore thought to arise from a sequence of inter-conversions between bend and splay character of the line defect. This leads to the model in Fig. 15(b), in which we postulate the existence of a “double splay wall” ( $\mathcal{S}, \mathcal{S}'$ ), in which  $\mathcal{S}$  and  $\mathcal{S}'$  coincide and which has the topological property that no net change in chirality is incurred when crossing it.

To account for the striking transverse modulations in stripe intensity associated with “jagged” defects in a consistent way, we find that the bond-director field model already introduced in Ref. [8] and reproduced in Fig. 10(b) must be augmented to include explicitly the effects of line defects on the bond-angle field, as discussed in the preceding section. Starting with the ansatz that the bond field is continuous through bend walls, we find that the existence of jagged line defects with no extra stripes requires the introduction of an average  $\pi/3$  phase slip [50] between bond-angle and director fields when crossing any bend wall, as indicated in the brick wall case of Fig. 10(c). A line defect comprising both bend  $\mathcal{B}$  and splay  $\mathcal{S}'$  segments is a single topological object that has the same action on the bond field everywhere along its length. The sign of the phase slip is correlated with the orientation of the cusp formed by the stripes where they intersect the line defect, or, equivalently, with the chirality of this intersection point. One phase slip of equal sign is introduced for each similar bend wall crossed by a given stripe. That is, the phase angle  $(\theta - \phi)$  continues to “wind up” as a stripe traverses an array of similar bend walls. The result, readily ascertained from inspection of Fig. 10(c), is the sampling of successive degenerate pairs,  $(L_1, L_2)$ , of chiral substates, each pair being associated with a different symmetry direction of the original bond-angle field. The topological charge acquired when crossing bend walls which generate cusps of one orientation can only be neutralized by crossing an equal number of bend walls with cusps of the opposite orientation. Thus, as implied in the model of Fig. 14(b), *crossing a closed loop leaves no net phase slip*.

The association of phase slip with line defects has an important consequence for the double splay wall considered above. Figure 12(b) showed how a newly emerging wall,  $\mathcal{S}'$ , while still corresponding to a splay wall for the

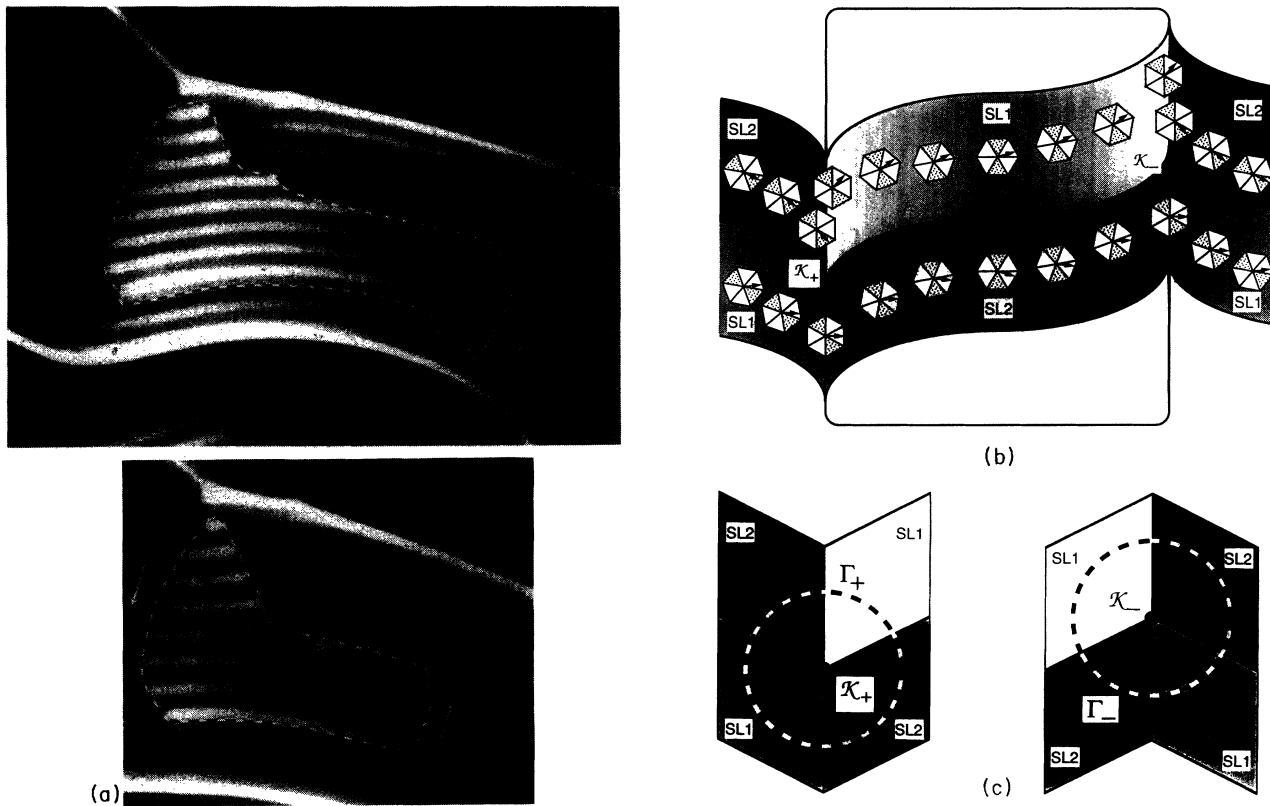


FIG. 14. Line defects as loops. (a) Closed loops in the stripe phase contract and become more rounded, ultimately shrinking to nothing. Note that the cusps in the stripe pattern adopt opposite orientations along the left and right boundaries of the loop, as indicated by the arrows. The horizontal dimension of the first frame is about  $160 \mu\text{m}$  and the elapsed time between frames about 30 sec. (b) Director-bond field associated with the intersections of stripes with two successive bend walls forming part of a loop, using the model of Fig. 10(c). (c) Schematic illustration of cusp orientation and stripe intensities at opposite intersection points of a stripe and transverse line defects forming part of a loop. The closed contours,  $\Gamma_-$  and  $\Gamma_+$ , enclosing, respectively, the intersection points  $\mathcal{K}_-$  and  $\mathcal{K}_+$ , must be followed in opposite direction senses, to realize identical sequences of stripe intensities (“colors”). This construction serves to define the chirality associated with each of the intersection points.

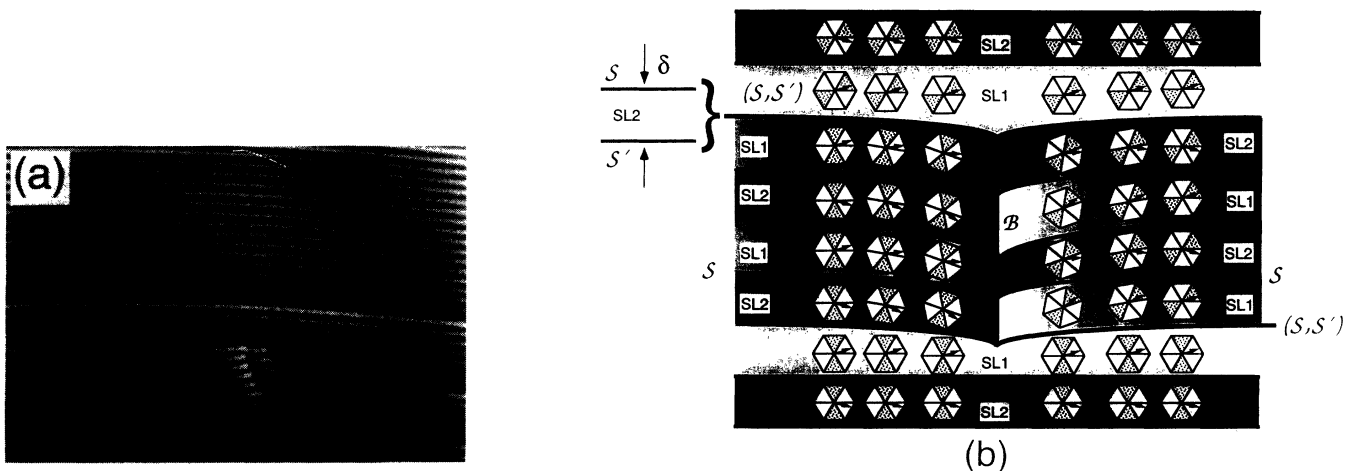


FIG. 15. Conversion of transverse to longitudinal defects. (a) Stripe pattern containing longitudinal and transverse line defects, the latter in a “jogged” configuration. The horizontal dimension is about  $250 \mu\text{m}$ . (b) Bond and director field configurations associated with a simple jogged line defect, constructed by applying the model of Fig. 10(c). The defect is shown to undergo a series of interconversions between transverse and longitudinal orientations, the latter implying the creation of sections of double splay wall,  $(\mathcal{S}, \mathcal{S}')$ . This double splay wall may be thought of as a narrow stripe domain of vanishing width  $\delta$  for the purposes of understanding the chiral topology. The phase slip between bond and director fields associated with the line defect is retained as the wall undergoes interconversions between transverse and longitudinal orientations and hence between bend and splay character. As a result, a splay wall  $\mathcal{S}'$ , or double splay wall  $(\mathcal{S}, \mathcal{S}')$ , which is formed by a line defect is always topologically distinct from the regular splay walls  $\mathcal{S}$  of the pristine stripe phase.

director field, inherits, from the bend wall  $\mathcal{B}$  to which it is connected, the topological effect of introducing a  $\pi/3$  phase slip between bond and director fields. We suggest that this distortion in the bond-angle field is retained in the double splay wall ( $\mathcal{S}, \mathcal{S}'$ ) [see Fig. 15(b)] and is the origin of the persistent discontinuity in stripe intensity visible in Fig. 15(a). Inspection of this figure shows that the jump to the “white” color at each double wall appears to remain absolutely stable and unchanged along the stripe-stripe interface, in a manner consistent with the type of topological excitation (or “kink”) of the bond field we postulate here. In the transverse direction, the intensity is seen to decay back to the normal levels obtaining in the unperturbed region in the top portion of the figure.

The foregoing discussion has explored some of the implications of chiral symmetry breaking for the topological nature of line defects in a chiral SL phase. The important conclusion that line defects may not terminate in interior points has provided the basis of the interpretation of several specific stripe configurations. We conclude this section with some remarks on the conversion of the “brick wall” pattern of Fig. 4(c) into the “honeycomb” pattern of Fig. 4(d). We note in particular that this conversion requires no topological transformation, but is achieved by merely displacing (and deforming) existing wall segments.

The brick wall pattern is composed of an array of transverse line defects of equal topological charge, as indicated by the identical orientation of the cusps at successive bend walls (see also Fig. 4 of Ref. [8]). A comparison of the model for this pattern [Fig. 10(c)] with the potential energy curves of Fig. 1(b) shows that the free energy of the interfaces formed by a given bend wall  $\mathcal{B}$  must alternate in successive stripe domains: interfaces characterized by a continuous variation in stripe intensity (gray) involve a small phase slip ( $\theta - \phi$ ) and a minimal distortion of the director field, in contrast to those marked by a visible transition in intensity (black  $\leftrightarrow$  white). We propose that this periodic variation in the energy of successive segments of a transverse line defect represents the driving force for the pattern transformation. As Fig. 16 indicates, the essential distortion facilitating the conversion of the brick wall into the honeycomb pattern is produced by simply extending the length of the low-energy (gray) sections of the bend wall at the expense of its high-energy (black-white) sections.

We expect the details of the forces on the director and bond-angle fields (which may be partly electrostatic in nature; see below) that drive the transformation of the curved brick wall segments into elongated hexagons to be subtle and not readily accessible to simple qualitative arguments. However, the fact that gray sections are indeed expanded while black-white sections are contracted relative to their originally identical lengths lends further support, in our view, to the essential ingredients of our model of the stripe phase.

## VII. DISCUSSION

In the foregoing sections we have presented a detailed description of the temperature-induced evolution of novel

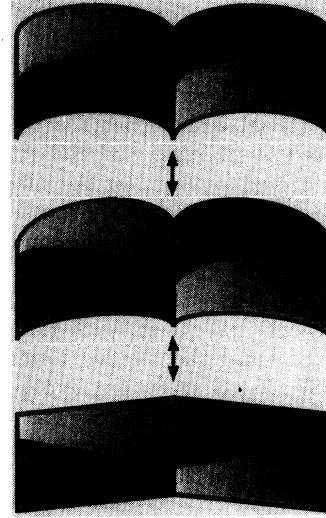


FIG. 16. Brick-wall-to-honeycomb transformation. Illustration of the relative elongation and contraction of successive bend wall segments in a brick wall pattern required as the essential mechanism of generating a honeycomb pattern like that in Fig. 4(d). The respective segments correspond to energetically different transitions between chiral substates  $L_1$  and  $L_2$ . What drives the originally curved stripe segments (the “bricks”) to transform to straight-sided structures is not known.

stripe textures observed in freely suspended films of non-chiral molecules which exhibit a phase transition from being uniform SC to having surface hexatic layers. We have invoked symmetry arguments to construct a model of the observed stripe phase as a chiral SL phase. This model, in the version originally introduced elsewhere [8], facilitates the detailed analysis of a variety of complex structures introduced in the stripe pattern by line defects, and provides a rationale for the observed transformation of brick wall into honeycomb patterns. The realization that broken chiral symmetry disallows point defects in a surface SL phase leads to the principal conclusion that line defects in our stripe phase must either end at the film boundary or form loops. The latter requires an interconversion between bend and splay character of the line defects. Our analysis culminated in the augmentation of the original model to include a phase slip between bond-angle and director fields at each such line defect. This augmented model was sketched in Fig. 12 and applied to line defects in Fig. 14.

The absence of a stripe phase in very thin films has a natural explanation within the framework of the model we have elaborated. Below a certain thickness, the film surfaces start to interact and the director  $\hat{n}$  is constrained to be *uniform* through the film [18].  $C_2$  rotation symmetry about the tilt plane normal is then restored, with the consequence that the SL is then no longer a chiral phase and stripe domain formation of the kind we are proposing would be inhibited. Alternatively, since the phase behavior of films of several LC materials, including 7O.7, shows a strong dependence on the number of smectic layers in the film [26], it may be that the surface SL phase

itself is suppressed below a certain thickness (in favor of, say, the SI).

The general sequence of hexatic textural changes seen in our films and, particularly, the striking similarity of the observed 12-armed stars in islands to the SL petal structure proposed by Selinger and Nelson [19] provide, in our view, additional support for our interpretation of the stripe phase. The fact that 12-armed stars transform reversibly to six-armed stars on cooling, as shown in Fig. 9, would also be characteristic of a SL-SF phase transition [19]. We might therefore tentatively identify the high-temperature line phase with the SI, the stripe phase with the SL, and the banded lower-temperature phase with the SF. X-ray scattering experiments testing this assignment are currently in progress.

Several additional observations give important clues as to the nature of the structures and phase transitions in our films. For example, the transverse (or radial) bend domain walls in our films are seen to exhibit substantial transverse fluctuations ("wall wandering") near the SC phase transition and they transform reversibly to broader SC brushes on heating. While quantitative analysis remains to be performed, these phenomena would be consistent with critical behavior, as predicted for SL bend walls by Selinger [17]. The observed broadening of the stripes with decreasing temperature is consistent with a general increase in the elastic stiffness, as has been observed in light scattering experiments on hexatic films [11,51].

In a "defect-free" striped film, the director orientation is simply alternating between two neighboring SL sub-states. Since the  $SL_1$  and  $SL_2$  states should have the same energy, it seems entirely reasonable that alternating stripes should be of the same width, and that all splay walls should have the same energy and width as one another. This would be consistent with our observations.

Whatever the actual thermodynamic phase of the striped films, a fundamental question concerns the molecular origin of the repulsive interaction stabilizing the array of walls. We believe that a contribution to such a term probably results from dipole-dipole interactions. X-ray measurements have revealed that in 70.7 films in the SI/SC phase, molecules closer to the surfaces are considerably more tilted than those in the interior [47]. According to Durand [52], a gradient in the magnitude of the nematic or smectic order parameter in the direction normal to the film-air interface generally induces an ordo-electric surface polarization. The tilt gradient experimentally observed in freely suspended films could therefore conceivably lead to a surface polarization in terms of this model.

In our films, below the SC-hexatic transition, we have argued that each hexatic surface layer at the liquid crystal-air interface exists in an asymmetric environment (bounded by the two fluids, air and SC-phase LC) which, given a finite molecular dipole moment, will generally result in a surface polarization [53]. Indeed, experiments on FTE1 films just above the hexatic transition do reveal a *polar* (rather than dielectric) response of the director field to weak applied electric fields ( $E \sim$  a few V/mm), which would seem to confirm the presence of permanent dipoles in the film. At lower temperature, however, the stripes

show no identifiable response to the same weak fields, which may be attributable to the film's increased hexatic stiffness. Continued attempts to reorient the stripes by increasing the applied field strength were made inconclusive by the onset of electroconvective flow.

We have also applied a dc magnetic field ( $B \sim 0.1$  T), inclined at about  $20^\circ$  to the film plane, while cooling from the SC phase. Although there appeared to be some initial ordering of freshly formed stripe domains near the film center, the final stripe orientation after cooling (by which time there was essentially a single set of stripes with few defects) was apparently determined primarily by strong boundary conditions at the edge of the film rather than by the field. Magnetic fields of this strength typically produce very good alignment of the director field in tilted hexatic films [11,51] and we do not understand why striped films should not respond in a similar fashion.

We note that although our stripe phase model derives continuing moral support from the ideas of Selinger and his co-workers, even their latest theory of modulated hexatic films [18], although predicting several interesting modulated structures in two dimensions, is as yet unable to account specifically for a texture of uniform SL stripes of the type we observe. While these may yet be discovered by a further exploration of phase space in their theory, we end by suggesting two areas of possible theoretical development concerning the existence of a surface polarization, which would generally have components both parallel and normal to the layer plane.

First, the existence of a normal polarization is expected to lead to pattern formation in a manner analogous to that obtaining in Langmuir monolayers adsorbed at an air-water interface. Stripe and hexagonal bubble domain patterns are found by theory to be the modulated phases of lowest free energy [2,54]. The competing contributions to pattern formation of this electrostatic interaction and of the elastic instabilities arising from chiral symmetry breaking may lead to rich and complex behavior.

Second, the very presence of a polarization, in addition to renormalizing elastic constants, may favor certain director configurations, both within each smectic layer and between successive layers. Here it is important to note that in principle, *all* LC interfaces to different material lack inversion symmetry and therefore allow the possibility of a spontaneous polarization parallel to the director at the interface. Such surface polarization has been detected, for example, in nematics at the LC-glass interface [55,56], and in tilted smectic phase films of racemic LC forming on the surface of isotropic droplets [53]. The possible importance of surface polarization effects in freely suspended films was addressed early on by Rosenblatt and co-workers in an effort to explain the unexpectedly high splay elasticity measured in SC films [25,57]. Calculations by Meyer and Clark showed that electrostatic interactions of surface molecular dipoles could indeed lead to an upward renormalization of the effective splay elastic constant, as observed [58]. Explicit theoretical consideration of hexatic ordering in the presence of such electrostatic interactions, certain to be present near any asymmetric interface, would clearly be of interest to further experiments on thin liquid crystal films.

## VIII. SUMMARY

We have described the spontaneous formation of modulated textures in hexatic films of nonchiral liquid crystal. A periodic stripe texture is identified as being domains of uniform director orientation separated from one another by splay walls which arise from the breaking of up-down symmetry by the polar hexatic surface layers. Additional long-wavelength modulations of the director field result in the appearance of linear grain boundaries in the bond-director orientation. An explicit model of the director configuration requires macroscopic rotations of the hexatic bond lattice, and the introduction of a chiral symmetry breaking consistent with that expected in the SL phase, with domain walls mediating changes in chirality. This assignment of SL symmetry is supported both di-

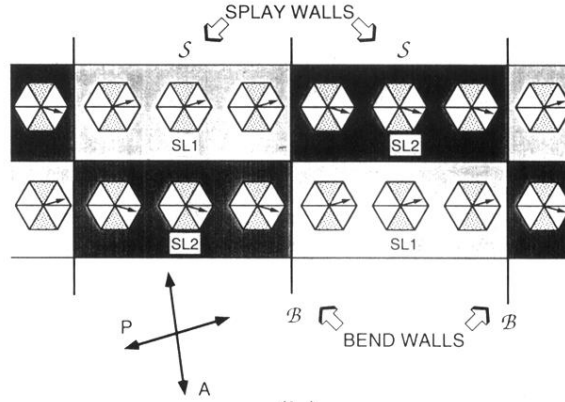
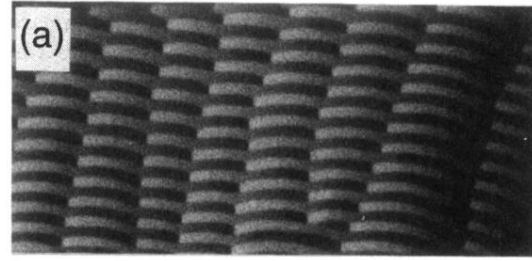
rectly by microscopic observations of textural transitions in the films which are characteristic of the SL phase, as well as indirectly by published x-ray data on other systems. Further x-ray and electron diffraction experiments are now being performed specifically to confirm the thermodynamic phase and probe the precise molecular ordering of the striped texture.

## ACKNOWLEDGMENTS

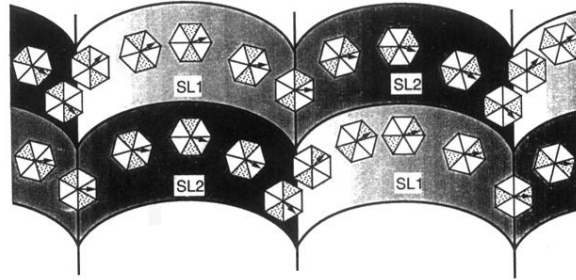
We wish to acknowledge enlightening conversations with J. Selinger, D. Walba, and R. Pindak, whom we also thank for lending us his magnet. This work was partially supported by NATO Collaborative Research Grant No. CRG 910141.

- 
- [1] T. Garel and S. Doniach, *Phys. Rev. B* **26**, 325 (1982); M. Seul *et al.*, *Science* **254**, 1616 (1991).
- [2] D. Andelmann, F. Brochard, and J.-F. Joanny, *J. Chem. Phys.* **86**, 3673 (1987); M. Seul and M. J. Sammon, *Phys. Rev. Lett.* **64**, 1903 (1990).
- [3] O. L. Alerhand, D. Vanderbilt, R. Meade, and J. D. Joannopoulos, *Phys. Rev. Lett.* **61**, 1973 (1988); D. Vanderbilt, *Surf. Sci. Lett.* **268**, L300 (1992).
- [4] C. D. Muzny, D. van Winkle, and N. A. Clark (cited in Ref. [5]).
- [5] S. A. Langer and J. P. Sethna, *Phys. Rev. A* **34**, 5035 (1986).
- [6] G. A. Hinshaw, R. G. Petschek, and R. A. Pelcovits, *Phys. Rev. Lett.* **60**, 1864 (1988); G. A. Hinshaw and R. G. Petschek, *Phys. Rev. A* **39**, 5914 (1989).
- [7] A. E. Jacobs, G. Goldner, and D. Mukamel, *Phys. Rev. A* **45**, 5783 (1992).
- [8] J. E. MacLennan and M. Seul, *Phys. Rev. Lett.* **69**, 2082 (1992); **69**, 3267(E) (1992).
- [9] E. B. Sirota, G. S. Smith, C. R. Safinya, R. J. Plano, and N. A. Clark, *Science* **242**, 1406 (1988); G. S. Smith, E. B. Sirota, C. R. Safinya, R. J. Plano, and N. A. Clark, *J. Chem. Phys.* **92**, 4519 (1990).
- [10] C. H. Young, R. Pindak, N. A. Clark, and R. B. Meyer, *Phys. Rev. Lett.* **40**, 773 (1978).
- [11] S. B. Dierker and R. Pindak, *Phys. Rev. Lett.* **59**, 1002 (1987).
- [12] S. B. Dierker, R. Pindak, and R. B. Meyer, *Phys. Rev. Lett.* **56**, 1819 (1986).
- [13] R. B. Meyer, L. Liebert, L. Strzelecki, and P. Keller, *J. Phys. (Paris) Lett.* **36**, L69 (1975).
- [14] R. B. Meyer and P. S. Pershan, *Solid State Commun.* **13**, 989 (1973).
- [15] F. C. Frank, *Discuss. Faraday Soc.* **25**, 19 (1958).
- [16] T. J. Scheffer, H. Gruler, and G. Meier, *Solid State Commun.* **11**, 253 (1972); C. Allet, M. Kléman, and P. Vidal, *J. Phys. (Paris)* **39**, 181 (1978).
- [17] J. V. Selinger, in *Complex Fluids*, edited by D. Weitz, E. Sirota, T. Witten, and J. Israelachvili (Materials Research Society, Pittsburgh, 1992), pp. 29–34.
- [18] J. V. Selinger, Z.-G. Wang, R. F. Bruinsma, and C. M. Knobler, *Phys. Rev. Lett.* **70**, 1139 (1993).
- [19] J. V. Selinger and D. R. Nelson, *Phys. Rev. A* **39**, 3135 (1989).
- [20] X. Qiu, J. Ruiz-Garcia, K. J. Stine, C. M. Knobler, and J. V. Selinger, *Phys. Rev. Lett.* **67**, 703 (1991).
- [21] X. Qiu, J. Ruiz-Garcia, and C. M. Knobler, in *Interface Dynamics and Growth*, edited by K. S. Liang, M. P. Anderson, R. F. Bruinsma, and G. Scoles, MRS Symposia Proceedings No. 237 (Materials Research Society, Pittsburgh, 1992), p. 263.
- [22] C. M. Knobler (private communication).
- [23] H. Möhwald, R. M. Kenn, K. Kjaer, and J. Als-Nielsen, in *Amphiphilic Membranes, Their Structure and Conformation*, edited R. Lipowsky, D. Richter, and K. Kremer (Springer, Berlin, 1992), pp. 9–18.
- [24] Instec Inc., P. O. Box 7246, Boulder, CO 80306.
- [25] C. Rosenblatt, R. Pindak, N. A. Clark, and R. B. Meyer, *Phys. Rev. Lett.* **42**, 1220 (1979).
- [26] E. B. Sirota, P. S. Pershan, L. B. Sorensen, and J. Collett, *Phys. Rev. A* **36**, 2890 (1987); E. B. Sirota, P. S. Pershan, S. Amador, and L. B. Sorensen, *ibid.* **35**, 2283 (1987).
- [27] C. Rosenblatt and N. M. Amer, *Appl. Phys. Lett.* **36**, 432 (1980).
- [28] G. Decher, J. MacLennan, M. Straus, and U. Sohling, *Makromol. Chem., Macromol. Symp.* **46**, 313 (1991). FTE1 is 5-(4''-hexyl, 3'-fluoro-*p*-terphenyl-4-oxy)-pentanoic acid ethyl ester.
- [29] 7O.4 is 4-(*n*-heptyloxy)benzylidene-4-(*n*-butyl)aniline; 5O.7 is 4-(*n*-pentyloxy)benzylidene-4-(*n*-heptyl)aniline; and 7O.7 is 4-(*n*-heptyloxy)benzylidene-4-(*n*-heptyl)aniline.
- [30] J. W. Goodby (private communication).
- [31] When Schiff's base films are kept for several hours in air at elevated temperature, there is a large shift in phase transition temperatures, and the optical contrast of stripes decreases markedly. It seems likely that the gradual buildup of hydrolysis products would eventually inhibit the striped phase altogether.
- [32] D. Demus and L. Richter, *Textures of Liquid Crystals* (Verlag Chemie, Weinheim, 1978).
- [33] J. Pang, C. D. Muzny, and N. A. Clark, *Phys. Rev. Lett.* **69**, 2783 (1992).
- [34] D. H. Lee and G. Grinstein, *Phys. Rev. Lett.* **55**, 541

- (1985).
- [35] S. Amador, P. S. Pershan, H. Stragier, B. D. Swanson, D. J. Tweet, L. B. Sorensen, E. B. Sirota, G. E. Ice, and A. Habenschuss, *Phys. Rev. A* **39**, 2703 (1989).
- [36] D. H. Van Winkle and N. A. Clark, *Phys. Rev. A* **38**, 1573 (1988).
- [37] G. W. Gray and J. W. Goodby, *Smectic Liquid Crystals—Textures and Structures* (Leonard-Hill, Glasgow, 1984).
- [38] The orientation of the disclination lines (normal to the former hexatic domains) is geometrically equivalent to that of the smectic layers which are oriented perpendicular to the needlelike smectic bâtonnets that form at the isotropic-SA transition in LC cells [37]. In fact, focal-conic defects are a common feature of many quasi-lamellar phases, similar textures also being exhibited, for example, by cholesteric LC [32].
- [39] Sometimes the line texture is not observed at all, in which case the grainy film texture evolves directly into the stripe phase.
- [40] M. Seul and R. Wolfe, *Phys. Rev. Lett.* **68**, 2460 (1992); M. Seul and R. Wolfe, *Phys. Rev. A* **46**, 7519 (1992); **46**, 7534 (1992).
- [41] A calculation by Van Winkle and Clark [36] of the three-dimensional (3D) director orientational correlations in a SC film, in the one-elastic constant approximation, yielded the following expression for the mean square orientation difference between the top and bottom of a film of thickness  $L$ :
- $$\begin{aligned}\sigma^2(L/2, -L/2) &= \langle |\phi(L/2) - \phi(-L/2)|^2 \rangle \\ &= \frac{4A}{(2\pi)^2} \int d^2q \sum_{\ell} \frac{2k_B T}{K(q^2 + q_{\ell}^2)} \\ &\quad \times \sin^2(q_{\ell}L/2),\end{aligned}$$
- where  $A$  is the area and  $D$  the longest dimension of the film, and  $K$  is a 2D Frank elastic constant. When just the lowest energy ( $\ell = 1$ ) mode is considered, for which  $q_{\ell} = \pi/L$ , we have
- $$\sigma^2(L/2, -L/2) = \frac{4Ak_B T}{(2\pi)^2 K} \int_{2\pi/D}^{2\pi/R} dq \frac{2\pi q}{q^2 + (\pi/L)^2},$$
- where the upper limit of the integral is set by the in-plane optical resolution distance  $R \sim 1 \mu\text{m}$ . For typical films,
- where  $L \ll R \ll D$ ,  $K \sim 4 \times 10^{-14}$  ergs, and  $k_B T \sim 4 \times 10^{-14}$  ergs, this yields  $\sigma^2 \sim (1/5\pi)(2L/R)^2$ , corresponding to an azimuthal deviation of  $\sigma_{\text{rms}} \lesssim (N/10)^\circ$  between the top and bottom surfaces of an  $N$ -layer film.
- [42] A. S. Farber, Ph.D. thesis, Brandeis University, 1986 (unpublished).
- [43] J. E. MacLennan, J.-Z. Pang, and N. A. Clark (unpublished).
- [44] See, for example, N. C. Bartelt, T. L. Einstein, and E. D. Williams, *Surf. Sci. Lett.* **240**, L591 (1990); E. D. Williams and N. C. Bartelt, *Science* **251**, 393 (1991).
- [45] D. H. Van Winkle, Ph.D. thesis, University of Colorado, 1984 (unpublished).
- [46] C. R. Walton and J. W. Goodby, *Mol. Cryst. Liq. Cryst.* **92**, 263 (1984). This texture is also shown in Plate 105 in Ref. [37].
- [47] D. J. Tweet, R. Holyst, B. D. Swanson, H. Stragier, and L. B. Sorensen, *Phys. Rev. Lett.* **65**, 2157 (1990).
- [48] S. Amador and P. Pershan (private communications).
- [49] G. Toulouse and M. Kléman, *J. Phys. Lett. (Paris)* **37**, L149 (1976).
- [50] Since the phase slip in  $(\theta - \phi)$  is alternately  $\pi/3 - 2\phi_L$  and  $\pi/3 + 2\phi_L$ , the phase slip is  $2\pi/3$  for every two walls, or an average of  $\pi/3$  per wall.
- [51] S. Sprunt, M. S. Spector, and J. D. Litster, *Phys. Rev. A* **45**, 7355 (1992).
- [52] G. Durand, in *Incommensurate Crystals, Liquid Crystals and Quasi-Crystals*, edited by J. F. Scott and N. A. Clark (Plenum, New York, 1987); G. Barbero, I. Dozov, J. F. Paliarne, and G. Durand, *Phys. Rev. Lett.* **56**, 2056 (1986).
- [53] Y. Galerne and L. Liebert, *Phys. Rev. Lett.* **64**, 906 (1990).
- [54] H. M. McConnell, *Annu. Rev. Phys. Chem.* **42**, 171 (1991); C. M. Knobler and R. C. Desai, *ibid.* **43**, 207 (1992).
- [55] P. Guyot-Sionnest, H. Hsiung, and Y. R. Shen, *Phys. Rev. Lett.* **57**, 2963 (1986).
- [56] S. Tripathi, R. G. Petschek, and C. Rosenblatt, *Phys. Rev. A* **45**, 3387 (1992).
- [57] C. Rosenblatt, R. B. Meyer, R. Pindak, and N. A. Clark, *Phys. Rev. A* **21**, 140 (1980).
- [58] R. B. Meyer and N. A. Clark (unpublished) — cited in Ref. [57].



(b)



(c)

FIG. 10. Brick wall texture. (a) Array of line defects in the form of bend walls, decorating a stripe phase in the linear geometry and leading to the appearance of an intensity pattern in the form of a brick wall. The stripe period is approximately  $12 \mu\text{m}$ . (b) Naive proposed smectic- $L$  bond and director fields for the brick wall texture in (a). Each lateral stripe boundary represents a splay wall which also mediates a change in SL chirality. Additional transverse line defects in the form of bend walls also mediate a change in SL chirality. The director field is nonuniform, bending along the stripes to give the characteristic observed intensities. (c) Refined version of the model in (b), in which a steady rotation of the bond field along the stripe direction results in an average  $\pi/3$  phase slip between bond and director fields for each crossing of a bend wall. The shaded hexagon segments labeling an arbitrary (but definite) symmetry direction of the hexatic lattice make the bond field rotation plain. The stripes curve to follow the lattice orientation, leading to the formation of cusps at the bend walls.

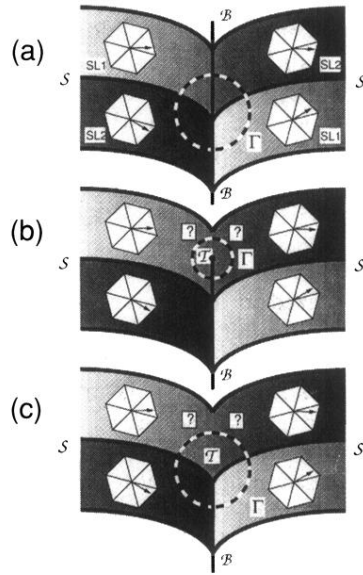
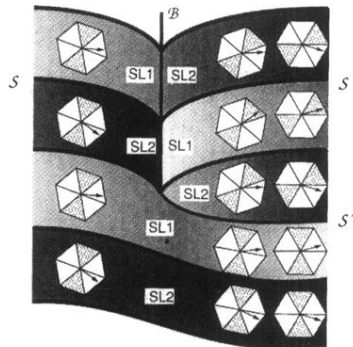
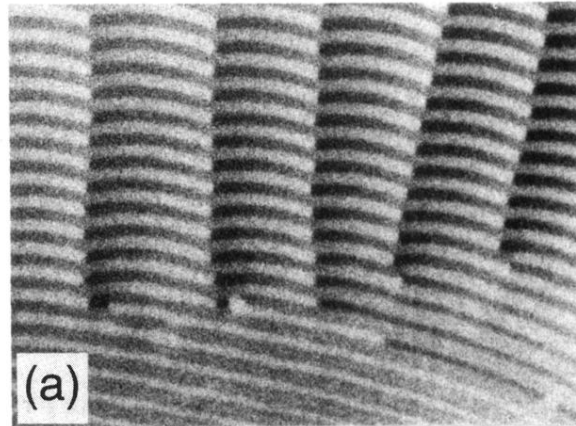


FIG. 11. Chiral topology of line defects in the stripe phase. (a) Details of bond and director fields, constructed for the surface of a SL film in accordance with the model of Fig. 10(b), at the intersection of a splay wall  $\mathcal{S}$  and a perpendicular bend wall  $\mathcal{B}$ . The intersection is characterized by a downward cusp in the stripe profile. Also shown is a contour,  $\Gamma$ , enclosing the intersection point. (b) and (c) illustrate arguments, given in the text, eliminating, respectively, the possibility of terminating a bend wall  $\mathcal{B}$ , either in the interior of a stripe, or at its intersection with a splay wall  $\mathcal{S}$ . The consequent ambiguity in the assignment of a chiral state near the hypothetical terminal point  $\mathcal{T}$  is indicated in both cases.



(b)

FIG. 12. Stripe dislocations terminating a bend wall texture. (a) Enlarged view of the apparent end points of the array of transverse line defects shown in Fig. 4(c). A dislocation in the stripe pattern is associated with each of the apparent end points. (b) Director-bond field model of the apparent terminal point of a transverse line defect  $\mathcal{B}$ , derived from that of Fig. 10(b). The model illustrates that the conversion of  $\mathcal{B}$  into an additional, distinct splay wall  $\mathcal{S}'$  requires the introduction of an edge dislocation in the stripe pattern.

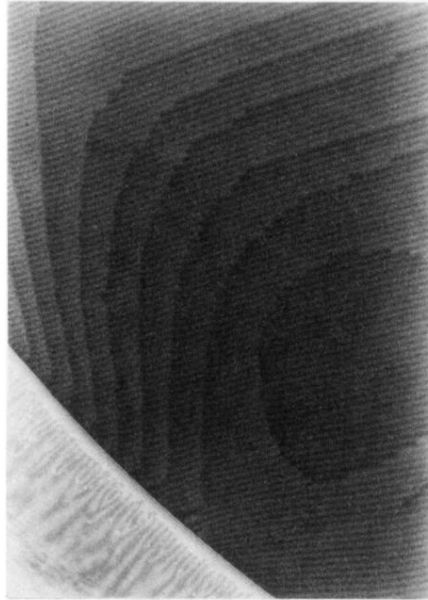


FIG. 13. Curved line defects. The photograph shows a stripe pattern permeated by an array of line defects emerging from the edge of the film (part of the filmholder is visible in the lower left portion of the image). Note that the cusps associated with successive defects adopt identical orientation (pointing upward). What are initially transverse line defects convert into longitudinal defects via “faceted” curved segments. A portion of a loop is visible in the lower right of the image. Details of the intensity modulations and cusp orientations are discussed in the text. The horizontal dimension of the field of view is approximately  $180\ \mu\text{m}$ .

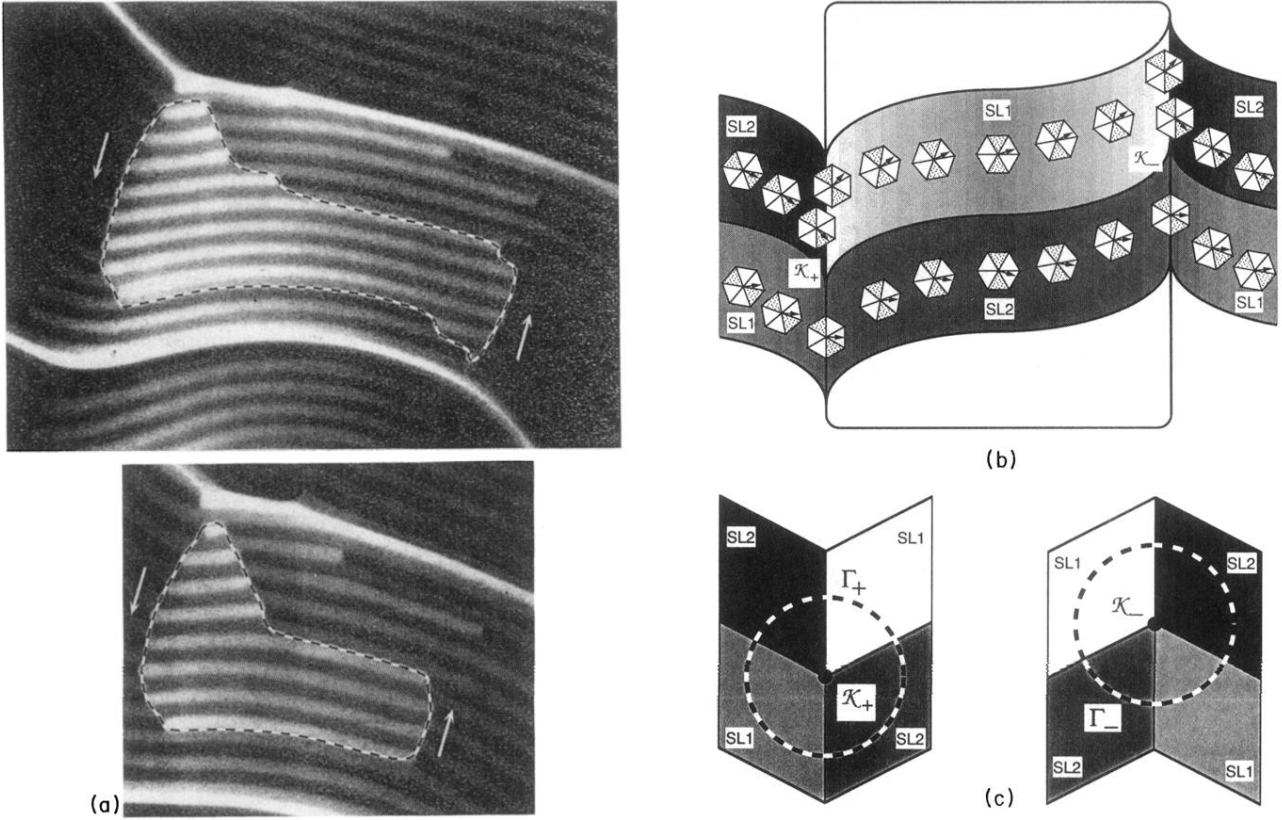


FIG. 14. Line defects as loops. (a) Closed loops in the stripe phase contract and become more rounded, ultimately shrinking to nothing. Note that the cusps in the stripe pattern adopt opposite orientations along the left and right boundaries of the loop, as indicated by the arrows. The horizontal dimension of the first frame is about  $160 \mu\text{m}$  and the elapsed time between frames about 30 sec. (b) Director-bond field associated with the intersections of stripes with two successive bend walls forming part of a loop, using the model of Fig. 10(c). (c) Schematic illustration of cusp orientation and stripe intensities at opposite intersection points of a stripe and transverse line defects forming part of a loop. The closed contours,  $\Gamma_-$  and  $\Gamma_+$ , enclosing, respectively, the intersection points  $\mathcal{K}_-$  and  $\mathcal{K}_+$ , must be followed in opposite direction senses, to realize identical sequences of stripe intensities (“colors”). This construction serves to define the chirality associated with each of the intersection points.

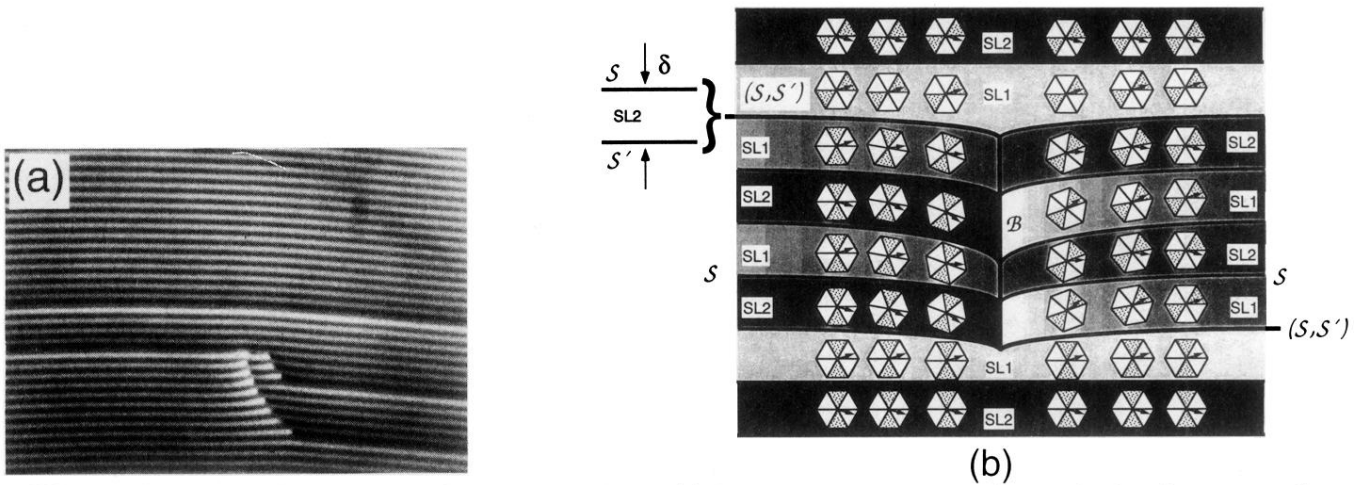


FIG. 15. Conversion of transverse to longitudinal defects. (a) Stripe pattern containing longitudinal and transverse line defects, the latter in a “jogged” configuration. The horizontal dimension is about  $250 \mu\text{m}$ . (b) Bond and director field configurations associated with a simple jogged line defect, constructed by applying the model of Fig. 10(c). The defect is shown to undergo a series of interconversions between transverse and longitudinal orientations, the latter implying the creation of sections of double splay wall,  $(\mathcal{S}, \mathcal{S}')$ . This double splay wall may be thought of as a narrow stripe domain of vanishing width  $\delta$  for the purposes of understanding the chiral topology. The phase slip between bond and director fields associated with the line defect is retained as the wall undergoes interconversions between transverse and longitudinal orientations and hence between bend and splay character. As a result, a splay wall  $\mathcal{S}'$ , or double splay wall  $(\mathcal{S}, \mathcal{S}')$ , which is formed by a line defect is always topologically distinct from the regular splay walls  $\mathcal{S}$  of the pristine stripe phase.

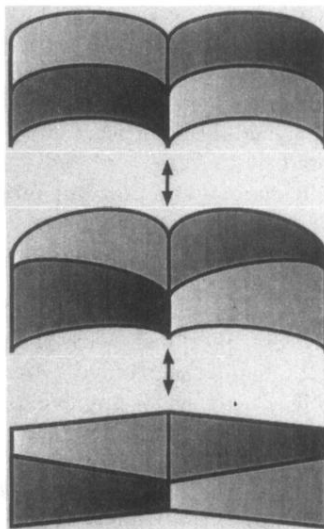


FIG. 16. Brick-wall-to-honeycomb transformation. Illustration of the relative elongation and contraction of successive bend wall segments in a brick wall pattern required as the essential mechanism of generating a honeycomb pattern like that in Fig. 4(d). The respective segments correspond to energetically different transitions between chiral substates  $L_1$  and  $L_2$ . What drives the originally curved stripe segments (the “bricks”) to transform to straight-sided structures is not known.

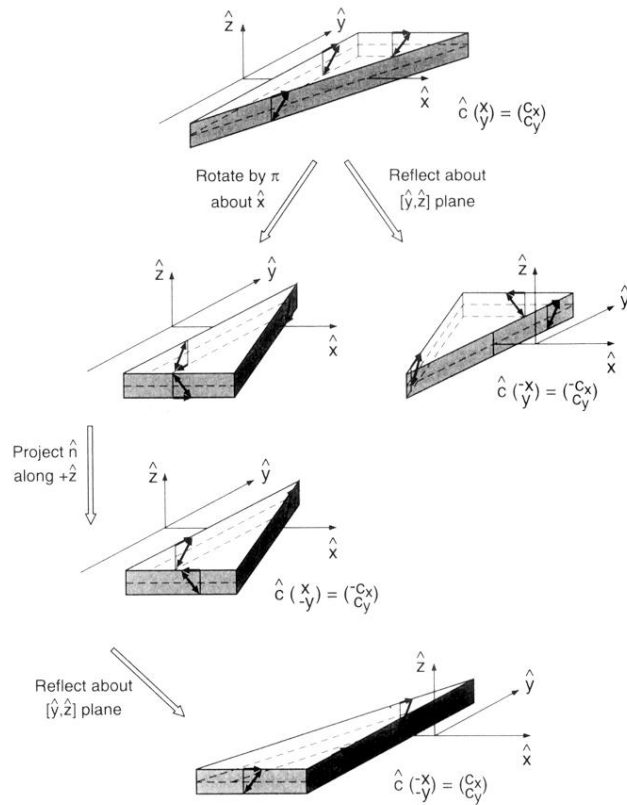


FIG. 2. Symmetry operations of tilted smectic films. This figure illustrates the transformation of  $\hat{c}$  under the  $C_2$  and  $\sigma$  symmetry operations shown in Fig. 1. The  $c$  director is by convention the layer-plane projection of the director  $\hat{n}$  chosen to have a component along the positive layer normal  $+\hat{z}$ .

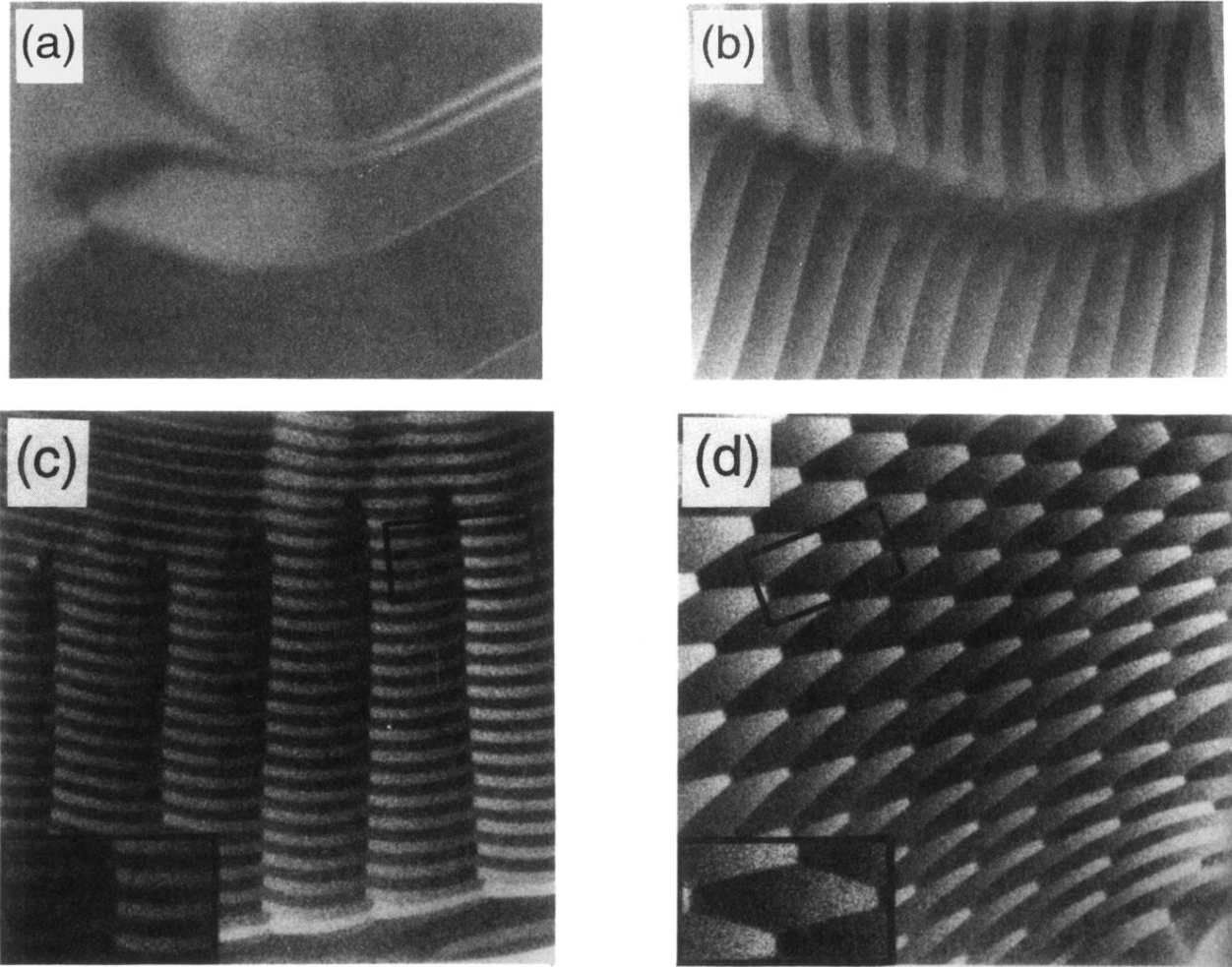


FIG. 4. Modulated textures in hexatic films. (a) Evolution of SC brushes to strings. The broad extinction brushes of the SC phase collapse to sharp strings when cooled to the hexatic phase transition ( $T \sim 80^\circ\text{C}$ ). When the film is subsequently heated, the inverse process, wall broadening, occurs. (b) Coexisting stripe and line texture in 7O.4 ( $T \sim 75^\circ\text{C}$ ). (c) Stripes near film edge, modulated by perpendicular line defects (brick wall texture). The stripes are bent into cusps at each line defect and can pass through only every second line unchanged ( $T \sim 73^\circ\text{C}$ ). (d) Honeycomb texture at low temperature ( $T \sim 65^\circ\text{C}$ ). The insets in (c) and (d) show details of the texture near bend walls. The horizontal dimension of (a) and (b) is about  $250\ \mu\text{m}$ , of (c) and (d) about  $130\ \mu\text{m}$ .

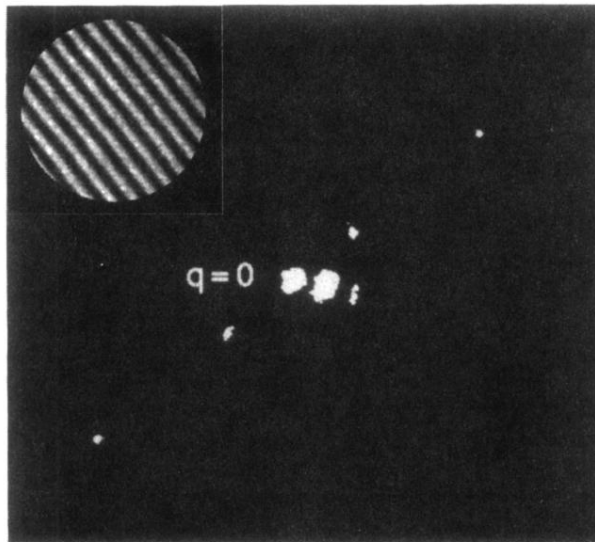


FIG. 5. Optical diffraction pattern from a striped film ( $T \sim 68^\circ\text{C}$ ). This computer-enhanced image shows the first and third order peaks as well as the central maximum. Fifth order spots were visible by eye but fell outside the imaging area of the camera. The two off-axis spots near the central maximum are stray reflections of the main beam; the even order peaks are absent. The inset shows a circular region of uniform stripes such as were illuminated in the diffraction experiment.

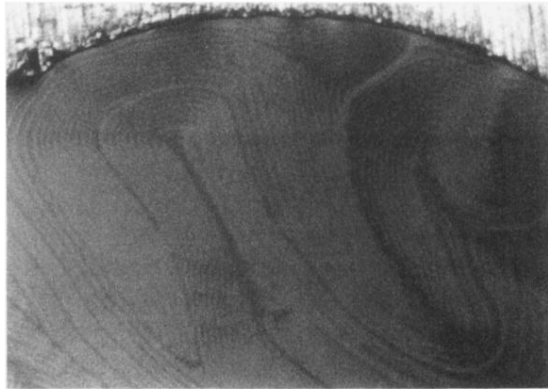


FIG. 6. Stripes buckling in response to rapid heating ( $T \sim 76^\circ\text{C}$ ). The horizontal dimension is about  $250\ \mu\text{m}$ .

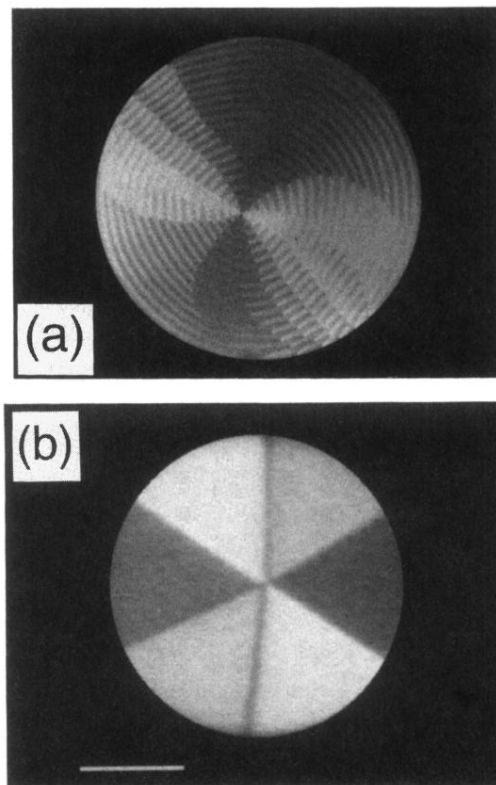


FIG. 7. Modulated hexatic textures in islands. (a) Concentric stripes modulated by a 12-armed star defect ( $T \sim 71^\circ\text{C}$ ). The horizontal dimension is about  $250\ \mu\text{m}$ . (b) Six-armed star defect at low temperature ( $T \sim 61^\circ\text{C}$ ). The surrounding film is considerably thinner and thus darker than the islands.

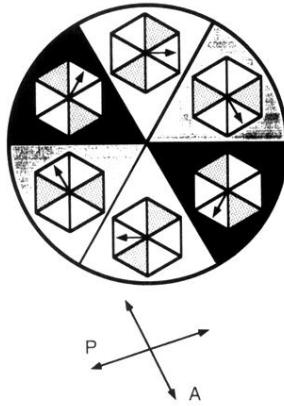


FIG. 8. Director field in a six-armed star. The  $c$  director is uniform in each sector and the six orientations shown here correspond to equilibrium azimuths of the SF phase. The polarizer and analyzer are decrossed, yielding three distinct reflection intensities. The bond orientation lattice rotates through  $|\Delta\theta| = 120^\circ$  in each arm, the shading of two segments of the lattice enabling visualization of its absolute orientation.

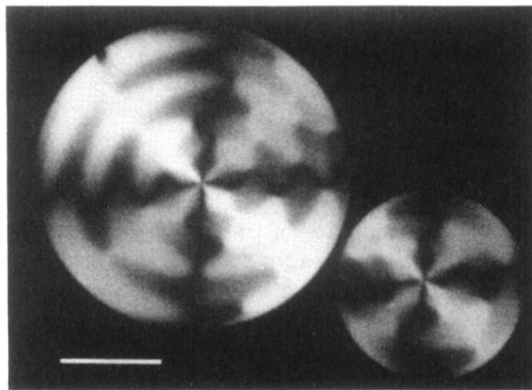


FIG. 9. Evolution of six- to 12-armed stars on heating ( $T \sim 64^\circ\text{C}$ ). The straight arms of the original six-armed star have destabilized and are no longer recognizable. On further heating, the irregular bulging domains seen in this picture extend circumferentially and reorganize into regular stripes modulated by a 12-armed star. The diameter of the larger island is about  $170\ \mu\text{m}$ .